Article:

Pantopoulos, G., Marini, M., Invernizzi, D. et al. (3 more authors) (2025) Quantification of internal heterogeneity across a submarine channel bend: a unique example from the late Tortonian Tachrift Channel Complex 5 (Taza–Guercif Basin, NE Morocco). Journal of Sedimentary Research, 95 (1). pp. 156-185. ISSN 1527-1404

https://doi.org/10.2110/jsr.2024.068

Quantification of the internal heterogeneity across a submarine channel bend: a unique example from the late Tortonian Tachrift channel complex 5 (Taza-Guercif Basin, NE Morocco)

George Pantopoulos,[1#*] Mattia Marini,[1] Daniele Invernizzi,[1] Imad El Kati,[2] Adam D. McArthur,[3] and Fabrizio Felletti[1]

[1] Department of Earth Sciences "Ardito Desio", University of Milan, Milan, Italy

[2] Natural Resources and Environment Laboratory, Polydisciplinary Faculty of Taza, Sidi Mohamed Ben Abdellah University, Taza, Morocco

[3] School of Earth and Environment, University of Leeds, Leeds, United Kingdom

[#] Present address: Department of Earth and Environmental Sciences, University of Pavia, Pavia, Italy

Corresponding author: georgios.pantopoulos@unipv.it

Keywords: *heterogeneity, facies, slope channel, lateral accretion package, outer bank bar, architectural element*

ABSTRACT

The heterogeneity of a deep marine slope channel complex is investigated through the acquisition of fifty sedimentary logs across three high-quality exposures of the late Tortonian Tachrift Complex 5, which constitutes part of the Neogene sedimentary infill of the Taza-Guercif Basin, NE Morocco. Various metrics extracted from log data (net-to-gross, amalgamation ratio, facies proportions, etc.) are processed to assess heterogeneity trends across the studied deposits. Sedimentological and stratigraphic analysis indicate that the exposures constitute upstream and downstream parts of a large-scale, left-turning channel bend. Sedimentary facies comprise different types of amalgamated sandstones, heterolithic and mud-rich sediments, grouped in channel-fill and overbank facies associations. Architectural elements recognized in channel-fill deposits are mainly lateral-accretion packages (LAPs), with additional elements recognized and recorded for the first time, representing different depositional settings across the channel bend, such as outer-bank bars and inner- to outer-bank transition bars. Analysis of heterogeneity metrics indicates the occurrence of two main types

of LAP, which vary depending on their upstream or downstream position across the bend, each with different internal heterogeneity (e.g., mean and lateral trends of net-to-gross, facies proportions, etc.) when compared with other elements deposited across the channel. The range and spatial arrangement of heterogeneity metrics observed could serve as an analog for assessing heterogeneity across channel bends of similar slope channel fills in the subsurface.

INTRODUCTION

Deep marine slope channel systems are large-scale (10's to 100's kms long and several to hundreds of meters thick) depositional units formed by sediments transported and deposited by powerful subaqueous gravity flows running down the continental slope (Mayall and Stewart 2000). They are usually formed down-slope of a submarine canyon, developing a series of stacked, spatially extensive and volumetrically large sand-rich deposits of channels, usually flanked by wedge-shaped related finer-grained overbank sediments (Walker 1975; Mutti and Normark 1987; Deptuck et al. 2003; Macauley and Hubbard 2013; Hubbard et al. 2014; Deptuck and Sylvester 2018; Hubbard et al. 2020). Slope channel systems are characterized by significant depositional complexity typified by the close juxtaposition of thick- to thin-bedded and coarse- to very fine-grained deposits (Macauley and Hubbard 2013; Hubbard et al. 2014; 2020; Tek et al. 2021; Bozetti et al. 2023). Complex internal architecture and geometries of channel-levee sediments are due to many reasons such as channel sinuosity and erosion, sediment type and grain size, flow intensity and rheological characteristics, slope grade and topography, tectonic setting, etc. (Kolla et al. 2007; McHargue et al. 2011; Sylvester et al. 2011; Janocko et al. 2013a; Jobe et al. 2015; Sylvester and Covault 2016; Crisóstomo-Figueroa et al. 2024).

Many contributions in geoscience research during recent years have been dedicated to slope channel systems, since in many cases their deposits are shown to host hydrocarbon reservoirs, and are also characterized by a great capacity for potential subsurface gas storage (Bruhn and Walker 1997; Weimer et al. 2000; Kolla et al. 2001; Prather 2003; Mayall et al. 2006). Large-scale slope channels also are the main pathways of sediment transfer from continental areas to the deep marine basins (Piper and Aksu 1987; Talling et al. 2007; Ruffell et al. 2024), hence their internal architecture and depositional characteristics are also of great interest for scientific research regarding environmental issues, such as submarine transfer and distribution of pollutants (e.g., microplastics) or organic carbon (McArthur et al. 2016; Kane and Clare 2019). Consequently, knowledge of the internal heterogeneity of slope channel systems is of importance in improving predictability and reducing uncertainty of crucial parameters (such as volume of possible reserves present, reservoir-body geometry, connectivity, and compartmentalization), especially when dealing with costly offshore cases of hydrocarbon exploration and/or carbon capture and storage (CCS) projects.

A particular feature of deep marine channels is their sinuous character (Kolla et al. 2007; Wynn et al. 2007), which creates extremely complex depositional sequences, formed by continuous lateral and/or downdip evolution of the channel (lateral accretion, channel sweep or swing) and also by the subsequent high aggradation rate of the whole submarine channel-levee depositional system, which is generally much larger than that observed in fluvial systems (Peakall et al. 2000; McHargue et al. 2011; Sylvester et al. 2011; Jobe et al. 2016). The size of resulting submarine channel bends due to sinuosity does show a scaling relationship with channel size, as in fluvial channels (Clark et al. 1992; Crisóstomo-Figueroa et al. 2024), but generally submarine channels tend to be wider than their fluvial counterparts (Pirmez and Imran 2003). However, the size and degree of sinuosity and the evolution of channel bends are also controlled by the main avulsion processes that drive the evolution of the submarine channel-levee system through time, and which can abruptly terminate channel development (Kolla 2007; Maier et al. 2013).

A large amount of field and subsurface-data studies during the last 30 years, along with recent advances in submarine imaging technology and geophysical instrumentation, allowed the scientific community to better observe a large variety of fine-scale depositional features both in and adjacent to (both ancient and recent) submarine channel deposits. These features range from thalweg scours, plugs and knickpoints to near-thalweg terraces and inner levees, along with features related to the channel-belt-bounding (outer) levee outside of the channel crest, like crevasse splays, sediment waves, splay lobes etc. (Clark and Pickering 1996; Deptuck et al. 2003; Babonneau et al. 2004; Deptuck et al. 2007; Nakajima et al. 2009; Hansen et al. 2015; Sylvester and Covault 2016; Kneller et al. 2020; Tek et al. 2022; Lobato et al. this volume). Additionally, regarding submarine-channel evolution and deposition around channel bends, specific trends of channel migration have been shown by several outcrop and subsurface studies, revealing a systematic trend of outer-bend erosion and inner-bend deposition with subsequent formation of laterally migrating and accreting deposits (Elliott 2000; Abreu et al. 2003; Lien et al. 2003; Arnott 2007; Kolla et al. 2007; Reimchen et al. 2016). Initial observations of laterally migrating deposits across submarine channel bends, mainly in seismic profiles and outcrop exposures, led to the introduction of the term lateral-accretion packages and/or deposits (LAPs or LADs, see also Abreu et al. 2003; Arnott 2007). These channel-fill deposits usually exhibit a general trend of gently dipping, coarse-grained, high net-to-gross and amalgamated sandstone and/or conglomeratic beds abruptly ending at a channel base, with finer-grained sediments on the one side (outer- or cut-bank), and interfingering with thin-bedded, low-density turbidites on the other (inner-bank) side (Arnott 2007). Several later studies have highlighted the wide variety and complexity of sedimentary facies that can be encountered in LAPs (Dykstra and Kneller 2009; Kane et al. 2009; Nakajima et al. 2009; Khan and Arnott 2011; Gamberi et al. 2013; Janocko et al. 2013a; Arnott et al. 2021; Tinterri and Civa 2021; Reguzzi et al. 2023; Zuffetti et al. 2023). Also, experimental studies have shown many differences in sedimentation near channel bends between submarine and fluvial channels, with the former creating a variety of bar-like deposits (apart from point bars) such as transition and counter or outer-bank bars (Straub et al. 2011; Janocko et al. 2013b; Peakall and Sumner 2015) and generally creating depositional bars in more downstream positions of the inner bend compared to subaerial fluvial channels (Peakall et al. 2007). Channel bends are categorized as either right-turning or left-turning, based on their downstream curvature direction. Regarding more complex terminologies related to channel bends, their constituent regions, and associated deposits, the terms inner and outer refer respectively to the point-bar side and the cut-bank side of a bend. The point of maximum curvature, known as the bend apex, separates the upstream and downstream regions of the bend (Janocko et al. 2013b). Transition zones, relatively broad areas where curvature gradually shifts across the inflection point, divide two successive bends with opposite curvatures. The term “bar” denotes a constructional (depositional) macroform that is approximately as long as the channel width and exhibits a positive topographic elevation relative to the channel thalweg (Nakajima et al. 2009). Following the classification by Janocko et al. (2013b), bank-attached bars are further identified as "point bars", "outer-bank bars", and transitional forms such as "inner-to-outer-bank" and "outer-to-inner-bank" bars, depending on their positional relationship with the banks. Additionally, outer-bank bars are subcategorized into "up-apex" and "down-apex" types.

Many previous studies have tried to assess the depositional and facies heterogeneity that can be encountered in submarine channel-levee deposits, especially towards quantitative characterization of observed facies, facies transitions, and depositional settings (Kane et al. 2007; Schwarz and Arnott 2007; Kane et al. 2009; Pringle et al. 2010; Pyles et al. 2010; Kane and Hodgson 2011; Funk et al. 2012; Moody et al. 2012; Macauley and Hubbard 2013; Nakajima and Kneller 2013; Hansen et al. 2015; Li et al. 2016; Morris et al. 2016; Hansen et al. 2017; Li et al. 2018; Fryer and Jobe 2019; Bell et al. 2020). However, internal heterogeneity of submarine-channel LAPs and related deposits accumulating at the bends of sinuous channels is still poorly constrained, although bar-like and laterally accreting deposit geometries appear to be very common in seismic imaging of subsurface analogues, with few published examples showing fine-scale quantitative facies patterns across deposits of submarine channel bends both in outcrop and in the subsurface (Nakajima et al. 2009; Babonneau et al. 2010; Pyles et al. 2010).

The wonderfully exposed outcrops of Channel Complex 5 belonging to the late Tortonian Tachrift Turbidite System, part of the Neogene infill of the Taza-Guercif Basin of NE Morocco (Felletti et al. 2020; 2023), offer an opportunity to document the lateral and vertical heterogeneity in an ~ 1-km-wide and 25-m-thick channel complex. The studied channel complex is comprising of a number of stratigraphic units which are interpreted to represent sediment accumulation across a large-scale channel bend that evolved through time (see also Marini et al., this volume). Fifty closely spaced logs of the outcrops provide a robust dataset of parameters such as bed thickness, grain size, net-to-gross, amalgamation ratio, facies proportions, etc., trends of which are observed across the studied deposits. Overall, the goal of the present study is to use this unique log dataset to provide documentation and quantification of internal heterogeneity patterns across both lateral (strike-oriented) or longitudinal (down-dip-oriented) transects of this large-scale submarine-channel bend. It is important to also note that the aim of this study is not to replicate every detail of the observed outcrop heterogeneity in static reservoir models. Instead, we focus on documenting key architectural and facies heterogeneity patterns that can inform the simplification and upscaling processes required for reservoir modeling. By identifying lateral and longitudinal trends, such as net-to-gross variability, facies proportions, and amalgamation ratios across a large-scale channel bend, we aim to highlight the critical elements that influence flow behavior.

GEOLOGICAL SETTING

The Rifian Corridor of NE Morocco (Flecker et al. 2015; Capella et al. 2018), represents a remnant of the Rif foreland basin, a large-scale structure which was part of a series of ancient relatively narrow seaways connecting the Atlantic Ocean to the Mediterranean sea during the late Miocene (Bernini et al. 1999; Gelati et al. 2000; Sani et al. 2000; Capella et al. 2017; 2019). At present, the Rifian Corridor is composed of the infills of three main sedimentary basins: the Gharb, Fes-Meknes and Taza-Guercif Basins (Fig. 1A). The latter was established in the early Tortonian as the result of flexural loading by the advancing thrust sheets of the Rif foreland, combined with concurrent reactivation of Middle Atlas tectonic structures (Bernini et al. 2000; Gelati et al. 2000; Sani et al. 2000; Capella et al. 2017).

In the area of the Taza-Guercif Basin (Fig. 1B), subsidence started in the late Tortonian (Krijgsman et al. 1999), resulting in marine transgression and accumulation of shallow marine deposits (Ras El Ksar Formation) locally overlying alluvial sediments (Draa Sidi Saada Formation, Benzaquen 1965; Bernini et al. 2000; Gelati et al. 2000), (Figs. 1B, C). The overlying Melloulou Formation (also referred as "Melloulou Unit", Gelati et al. 2000), represents the culmination of transgression and the maximum deepening of the basin, and is consisting of a succession of interbedded hemipelagic marlstones and turbidites (Bernini et al. 1999; Gelati et al. 2000; Sani et al. 2000; Krijgsman and Langereis 2000). The subsequent closure of the Rifian Corridor during the early Messinian led to a tectonically controlled regression, successive shallowing, and final emersion of the Taza-Guercif Basin (Krijgsman et al. 1999; Krijgsman and Langereis 2000; Capella et al. 2017; 2018), typified by deposition of the upper “Gypsiferous Marls Subunit” of the Melloulou Formation (Gelati et al. 2000) and of the overlying shallow marine to continental Kef Ed Debe Formation (Sani et al. 2000).

The Tachrift Turbidite System

In the southern part of the Taza-Guercif Basin, Melloulou Formation turbidite deposits crop out to the west and east of the Zobzit river, forming two distinct turbidite systems, the El Rhirane and the Tachrift systems respectively (Gelati et al. 2000) (Fig. 1B). Recent provenance studies indicate that both turbidite systems had a southernly located source originating from the Middle Atlas area (Pratt et al. 2016). The stratigraphic relationship between these two turbidite systems is still poorly understood, due to recent cover and presence of faults (Fig. 1B), but based on their lateral relationship and structural reconstructions, it was suggested that the El Rhirane system is probably older (Gelati et al. 2000).

The Tachrift system is composed of a ca. 600-m-thick turbidite succession (Fig. 1C) of alternating channelized turbidites and hemipelagic marlstones (Bernini et al. 1994; Gelati et al. 2000; Felletti et al. 2020). Magnetostratigraphic and biostratigraphic studies conducted in the area during the late 1990s (Krijgsman et al. 1999; Krijgsman and Langereis 2000) indicate that Tachrift system sediments were deposited within a time frame between 7.7 and 7.2 Ma with an increasing accumulation rate from late Tortonian to early Messinian. Krijgsman et al. (1999) initially recognized fifteen main turbidite layers in the Tachrift system which have been recently remapped as nine channel-levee turbidite complexes (*sensu* Gardner et al. 2003) (Fig. 1C) by Felletti et al. (2020). These complexes are interpreted as the depositional product of several turbidite channel belts developed along the southern bounding slope of the Taza-Guercif Basin. The ca. 25-m-thick Complex 5 occurs among these channel complexes, at the middle part of the Tachrift system stratigraphy, which is considered to have a late Tortonian age as indicated by magnetostratigraphy (Krijgsman and Langereis, 2000). Complex 5 sediments can be observed along a ca. 1-km-long series of very well exposed outcrop transects east of the Zobzit river, exhibiting a bipartite stratigraphy (Fig. 2), consisting of a lower ca. 20-m-thick main sand-rich channel body (which is the focus of the current study) and an upper mud-rich interval into which three thin-bedded sandstone bedsets are intercalated. A main paleoflow trend towards the N-NE (perpendicularly oriented to the outcrops) is observed along Complex 5 (Marini et al., this volume), also recorded in recent studies of Tachrift system sediments (Felletti et al. 2023; Reguzzi et al. 2023).

METHODS

Field Logging and Data Collection

Tachrift Complex 5 channel-levee deposits are investigated by acquiring and correlating around fifty closely spaced (average spacing is ca. 50 m) sedimentary logs from three main outcrops (Figs. 1D, 2). Log measurements were performed by making a combined use of a tape measure for individual bed thicknesses and a Jacob's staff with laser sighting capability (Patacci 2016) for thicker and/or mud-rich log intervals. Log descriptions are made until a cut-off thickness of 1 cm, and included information such as bed thickness, lithology, estimation of grain size (using a comparator and a hand lens), type of sedimentary structures, paleoflow directions from sole marks and ripple marks, oxidation, and bioturbation intensity. In the thicker-bedded and coarser parts of the studied channel-levee succession, characterized by frequent presence of amalgamation surfaces (sandstone-on-sandstone erosional contacts), boundaries of separate event sandstone beds were carefully identified by detecting characteristic grain-size changes and erosional features (Sylvester 2007; Pantopoulos et al. 2018). Stratigraphic logs are correlated by walking out event beds between adjacent localities. Correlations of sedimentary bodies across different outcrops (where physical correlation through walking along beds is impossible) is based on their stratigraphic position relative to a distinctive and laterally continuous turbidite bed occurring close to the base or, alternatively, to the midpoint of a channelized bed set located a few meters above the top of the main part of the studied channel-levee complex (bed set 5.1 in Fig. 2). The collected graphic logs were subsequently digitized using a drawing software and extraction of quantitative data (bed thickness, grain size, etc.) is performed using EasyCore® digital core-description software.

Heterogeneity Metrics

A range of parameters were calculated using field logging data, to investigate the internal heterogeneity of the studied channel-levee complex, which included i) bed thickness, ii) mean and basal grain size, iii) facies thickness proportion, iv) net-to-gross, v) amalgamation ratio, and vi) thickness percentage of mud intraclast horizons. Bed thickness data was obtained from measurement of logged sandstone and mudstone bed thicknesses to a resolution of 1 cm. The term "bed" used by the present study refers to the sandstone or mudstone lithological part of a turbidite measured in the field, and not to the overall depositional turbidite, which potentially grades from sand to silt and then to mudstone, which is referred as a "turbidite event". For each log, grain-size data originating from the basal part of each bed, as well as from successive grain-size measurements at 1 mm intervals from the base to the top of each event bed (using EasyCore log digitizing software) is used to calculate a range of basal and "bed mean" grain-size data for every bed, the variability of which in a log interval is later analyzed. Similar techniques of log digitizing and data extraction were also recently proposed by Jobe et al. (2021). Proportions of sedimentary facies are also investigated, determined as stratigraphic thickness percentage of the observed facies (defined by sedimentological characteristics during logging) in a particular stratigraphic interval. Details regarding types of facies observed in the field and their classification can be found in the following sections. The percentage of total sandstone thickness to total stratigraphic thickness for each log is calculated and will be referred as net-to-gross based on similar terminology used in previous works regarding heterogeneity of deep marine turbidite deposits (Fryer and Jobe 2019; Kus et al. 2022). Net-to-gross trends can be useful for observing vertical and lateral trends in sand content (Macdonald et al. 2011; Kus et al. 2022). Amalgamation ratio is determined as percentage transformation of the ratio of number of amalgamation surfaces divided by the total number of event beds in a given stratigraphic interval (Romans et al. 2009). Another logging parameter that is quantified and processed is the thickness of mud-intraclast-rich horizons (mud-clast breccias as well as mud-clast concentrated layers incorporated in many sandstone beds) in sand-rich intervals of the studied sediments, expressed as the percentage of the ratio of total mud-clast-layer thicknesses divided by the total stratigraphic thickness in a studied interval. The above parameters were statistically processed and plotted utilizing box-and-whisker plots (especially for measurements of bed thickness and grain size for illustrating median values and distribution variability), simple biplots (for net-to-gross, amalgamation ratio and mud-intraclast horizon-thicknesses) and stacked-bar charts for highlighting variability of facies thickness proportion. Plotting and analyses are performed using R Statistical Software (v4.2.2; R Core Team 2022).

RESULTS

Stratigraphic Units

Complex 5 is exposed along a ca. 1-km-long outcrop belt consisting of three main outcrops, which in the following text will be referred to as North, Southwest, and Southeast Outcrops (Figs. 1D, 2, 3). The main exposure of Complex 5 is best observed along the North Outcrop and is subdivided into four main stratigraphic divisions (which will be further referred as Units) based on major erosional surfaces, large-scale vertical changes in sedimentary facies, and lateral stratigraphic relationships (Fig. 2). Limits of stratigraphic Units are propagated from the North to Southwest and Southeast Outcrops, based on stratigraphic correlations and larger-scale stratigraphic relationships observed between the units. Groups of beds across the complex with similar sedimentological characteristics are classified as similar sedimentary facies (Table 1), which in turn are grouped in larger facies associations, each containing a range of architectural elements (Fig. 4, see also Marini et al., this volume).

Sedimentary Facies

Based on bed thickness, grain size, and sedimentary structures, seven main sedimentary facies (F1-F7) are identified in Complex 5 that are related with depositional processes and the classical facies schemes for turbidite and sediment-gravity-flow deposits proposed by Bouma (1962), Lowe (1982), and Mutti (1992). The main sedimentary and outcrop characteristics of the seven identified facies are briefly described and presented in Table 1.

Facies Associations and Architectural Elements

Based on bed correlations and depositional geometries (Fig. 3; see also Marini et al., this volume), the recognized sedimentary facies are grouped into seven facies associations (FAs) representing parts of channel-fill (FA1-FA5) and overbank architectural elements (FA6, FA7). Facies associations are composed of groups of individual beds with similar sedimentological characteristics and organized by decreasing sandstone bed thickness and grain size (Figs. 4, 5, 6). These are i) mud-clast-rich channel-fill sandstones (FA1), ii) trough-cross-stratified channel-fill sandstones (FA2), iii) sand-rich channel-fill heterolithics (FA3), iv) mud-rich channel-fill heterolithics (FA4), v) channel-margin deposits (FA5), vi) proximal overbank deposits (FA6), and vii) distal overbank deposits (FA7).

The four genetic units identified across the complex (labelled 1 to 4, from older to younger) range from a few meters to several meters in thickness and could be also identified in the Southwest and Southeast Outcrops (Fig. 2) based on their stratigraphic position relative to one or more datum planes, major erosional surfaces, and major changes in facies composition.

Unit 1 --- The Unit is composed mainly of channel-fill facies associations (FA2, FA3) which pass rapidly into nonchannelized muddy overbank facies (FA6) at more eastward localities (24-25 and 62-63 at the North and Southwest Outcrop respectively, Fig. 2). Channel-fill FAs (especially between localities 17-20 and 67 to 65) are composed of laterally accreting bed sets reflecting sediment accumulation at the inner bank of a meandering channel (*sensu* Abreu et al. 2003; Li et al. 2016; see also Marini et al., this volume). Since the observed bed sets exhibit an east- to southeast-directed accretion trend, and the main paleocurrent direction is towards N-NE, the accumulation of Unit 1 deposits in a bar at a left-turning bend of a channel is deduced. Mud-rich facies adjacent to the eastern margin of the latter channel are probably part of a levee that gradually created a muddy sediment buildup at the outer bank of the channel bend.

Unit 2 --- Deposits of this unit are composed mainly of channel-fill facies associations consisting of amalgamated to non-amalgamated sandstones (facies FA1, FA2, and FA5). Similarly to the underlying Unit 1, these channel-fill FAs pass laterally into muddy overbank deposits (FA6) at more eastern localities of both the North and Southwest Outcrops, where probably a levee depositional setting had been established (Marini et al., this volume). At Southwest Outcrop localities, (where the unit is not well-preserved due to erosion), Unit 2 is composed mainly of thick- to medium-bedded, amalgamated sandstones with deeply scoured bases. Due to the latter, is difficult to infer if these deposits are laterally accreting. In contrast, Unit 2 at North Outcrop localities is characterized by well-stratified, thick-bedded facies which exhibit a sigmoidal cross-sectional profile and aggradational geometries. The latter observations suggest that this Unit at North Outcrop areas may represent deposits of a bar developed at the outer bank of a left-turning channel bend (Marini et al., this volume), similar to larger-scale features observed mainly in the subsurface by previous studies (Nakajima et al. 2009).

Unit 3 --- The bulk of Unit 3 sediments is made up mostly of channel-fill facies associations (Fig. 4) which are laterally replaced by non-channelized, muddy facies associations (FA6) at more eastern localities (Fig. 2). These muddy FAs are probably in continuity with underlying muddy levee facies observed for Units 1 and 2. A general migration trend towards the east-southeast is observed for Unit 3 channel-fill facies associations at Southwest Outcrop localities (Fig. 3C), largely orthogonal to the main paleoflow, suggesting a similar migration of the channel pathway, which correlates with the accumulation of laterally accreting deposits at the southeastern part of the North Outcrop (especially between localities 27 and 30, Fig. 3B). The latter observations suggest possible accumulation of Unit 3 deposits onto the accreting inner bank of a left-turning channel bend in continuity with underlying units (Marini et al., this volume).

Unit 4 --- This Unit is characterized by both channel-fill and overbank facies associations (Fig. 4) with the former exhibiting laterally accreting deposits, implying its deposition in a meandering, leveed-channel setting probably established to the east-southeast of underlying channel-filling deposits (Marini et al., this volume). Deposition of this unit probably occurred on a pre-existing channel topography and represents a major reorganisation of the channel system towards the east-southeast after a major erosional phase (Marini et al., this volume).

Depositional Evolution

Fieldwork observations combined with previous sedimentological interpretations indicate that observed deposits of channel-fill facies associations of Channel Complex 5 probably represent a range of bar-like deposits formed across the bend of a meandering sinuous channel (Marini et al., this volume). In order to determine the type of depositional setting across the channel's bend, various information such as paleoflow trends as well as accretion directions and levee location in relation to the channel's pathway are utilized, and a paleogeographic reconstruction of the channel's complex evolution through deposition of Units 1 to 4 is created (Fig. 7; for more details see also Marini et al., this volume). The proposed evolutionary model incorporates the deposits of Units 1-3 at Southwest and North Outcrop localities as upstream and downstream parts respectively of a large-scale left-turning channel bend. Depositional scenarios for the evolution of Unit 4 (which reflects the final stages of the evolution of Complex 5) were also considered in the proposed evolutionary model (Fig. 7), but since its deposits are poorly preserved it is not further discussed in this work.

Descriptive Statistics of Fieldwork Logging

Fieldwork logging involved the detailed description of more than 2400 sandstone and 1600 mudstone beds respectively for all studied outcrops across Tachrift Complex 5 (Table 2). Mean sandstone thickness ranges from 10 to 22 cm depending on the stratigraphic unit (Table 2), with a maximum observed thickness of 200 cm. Mean mudstone thickness ranges between 7 and 17 cm with a maximum of 260 cm (mainly observed locally at the upper stratigraphic levels of the complex). The mean basal grain size of sandstone is medium sand, ranging between 0.3 and 0.4 mm for all studied logs (Table 2). In general, there is a decrease in mean sandstone thickness as well as sandstone thickness variance and basal grain size, from upstream (Southeast and Southwest) to downstream (North) outcrops for all Units except Unit 2, which exhibits an opposite trend (Table 2). In contrast, mean mudstone thickness as well as thickness variation shows a more complex pattern of downstream increase for Units 2 and 4, a downstream decrease for Unit 3, while mudstone thicknesses for Unit 1 show a stable downstream trend (Table 2). Regarding specific trends for the whole stratigraphic units, a tendency for the lower three units of having thicker and coarser sandstone and thinner mudstone beds is observed, in relation with the upper stratigraphic unit (Unit 4) which is generally more thin-bedded and finer in grain size (Table 2). Unit 2 exhibits larger values of mean sandstone thickness (~ 22 cm), thickness variance, and basal grain size, as well as lower values of mudstone thickness and variation in relation with Units 1 and 3.

Patterns of Internal Heterogeneity

Besides general trends in descriptive statistics of logging data (bed thickness, grain size, etc.), tendencies in sedimentary heterogeneity metrics such as net-to-gross, amalgamation ratio, mud-clast-horizon thickness and facies proportions are also explored. These tendencies are observed i) for the whole stratigraphic Units, ii) across individual stratigraphic Units, and for iii) contained architectural elements respectively. The analysis of the tendencies across Units will be focused on Units 1-3 (and their architectural elements) which constitute the bulk of Tachrift Channel Complex 5 sediments and mainly represent sedimentation across different settings of a slope-channel bend (Marini et al., this volume).

General Heterogeneity Trends for Stratigraphic Units ---

Net-to-gross and related metrics: Internal heterogeneity metrics based on simple ratios show variable trends across the studied channel complex for both upstream and downstream outcrops. The four stratigraphic units observed exhibit differences in heterogeneity patterns, with Unit 2 having larger values of net-to-gross and amalgamation ratio, along with more abundant occurrences of mud-clast horizons compared with the other packages (Table 3). In general, mean values of net-to-gross, amalgamation ratio, and mud-clast-horizon thickness seem to decrease downstream in all stratigraphic units. More particularly, mean net-to-gross (NG) ranges from ~ 60 to ~ 85% in upstream outcrops to the south, decreasing to a range of 25-80% in northern downstream outcrops, with Unit 4 exhibiting the lowest values. Amalgamation ratio (AR) is characterized by elevated mean values in southern outcrops (~ 28-68%), decreasing to a range of ~ 10-40% in the north (Table 3). Mean mud-clast-horizon thickness percentage (MHTP) ranges from ~ 5 to 23% in the south, diminishing to ~ 0.9-7.6% in northern more distal outcrops (Table 3). Regarding the distribution of heterogeneity metrics, boxplots of calculated values both for all outcrops studied and individual units respectively, show different tendencies for stratigraphic units sampled (Fig. 8). More particularly, Unit 2 shows higher median NG with smaller variations (at least for the 25th to 75th percentile) along with significantly elevated and variable AR and MHTP values, while both Units 1 and 3 exhibit medium to high NG (characterized by larger values and variation for Unit 3), accompanied with noticeable variation in AR values and MHTP occurrence (especially for Unit 3). Unit 4 displays lower and less variable NG, AR, and MHTP apart from southern more proximal outcrops, which show a rather elevated and variable AR pattern (Fig. 8).

Facies: Spatial and lateral distribution of sedimentary facies associations is observed through the creation of a stratigraphic panel with correlated FAs between logs (Fig. 9). The increased abundance of channel-fill sandstone FAs (FA1, FA2, and FA5) at the upstream Southwest Outcrop (especially for Units 2 and 3) can be visually observed, along with an additional increased abundance of sandy amalgamated FAs at the SE part of the downstream North Outcrop (Fig. 9). Heterolithic FAs (FA3 and FA4) are more abundant at the NW part of the North Outcrop (Fig. 9). Variation in facies observed is also explored based on data from all outcrops studied. Boxplots of variation based on facies thickness percentages from each log (Fig. 10A) display different trends between stratigraphic units: Units 1 and 3 show larger variation in thickness proportion both in mud-rich and in sand-rich channel-fill heterolithics (FA3 and FA4) as well as in trough cross-stratified channel-fill sandstones (FA2) and channel-margin facies (FA5). Unit 3 also exhibits large variation of proximal overbank FAs (FA6) and an abundance of mud-clast-rich channel-fill sandstones (FA1) in relation to Unit 1. Unit 2 is characterized by a significantly larger abundance and variation in mud-clast-rich channel-fill sandstones (FA1), as well as larger thickness proportions of channel-margin sandstones (FA5). Unit 4 is dominated mainly by trough cross-stratified channel-fill sandstone facies (FA2) and exhibits the larger thickness proportions of overbank facies (FA6). The previous observations are also validated by pie charts showing the mean FA percentage for each stratigraphic unit (Fig. 10B).

Heterogeneity trends across stratigraphic Units 1-3 ---

Unit 1: At the more proximal Southwest Outcrop, Unit 1 shows a gradual decrease in sandstone thickness towards the E-SE, along with a concurrent increase in mudstone thickness and variation respectively. Grain size also follows a decreasing trend towards the E-SE, along with net-to-gross (NG), amalgamation ratio (AR) and mud-clast horizon thickness-percentage (MHTP) values (Fig. 11). Facies-thickness proportion displays a main presence of trough cross-stratified sandstone (FA2) at the western logs (with more than 40-50% thickness proportion) with subsequent dominance of sand-rich channel-fill heteroltihics (FA3) towards the E-SE. Sandstone thickness at North Outcrop also shows a decreasing trend towards the ESE, but with elevated values at the central parts of the outcrop (logs 17-20, Fig. 12). The same trend holds also for grain size, which is also elevated around logs 24-26 (probably due to log incompleteness of poorly exposed lower thin-bedded parts). Net-to-gross displays a slight increasing pattern moving from western to more eastern logs, until a more stable trend appears (with values above 50%) before quickly diminishing to the east (after log 25, Fig. 12). AR shows elevated values at the central part of the outcrop again diminishing towards the east, while MHTP increases especially near eastern logs, before completely diminishing (Fig. 12). Facies proportions are dominated by sand-rich channel-fill heterolithic facies (FA3) at the western part of the northern outcrop, passing to more trough cross-stratified and channel-margin facies (FA2 and FA5) to the central and eastern part, with overbank facies (FA6 and FA7) completely dominating at the eastern edge of the outcrop (Fig. 12).

Unit 2: At more proximal settings (Southwest Outcrop), Unit 2 exhibits more elevated values of median sandstone thickness (ranging between 10 and 50 cm) and thickness variation compared with the underlying Unit 1, while mudstone thickness is characteristically low, with an exception at the eastern part of the outcrop. The Unit is also characterized by coarser sediments, with basal sandstone grain size ranging between medium and coarse sand (Fig. 11). NG displays large values (close to 100%) and is rather stable across the outcrop, diminishing to the east. AR and MHTP are also larger (with values of more than 50% and around 25% respectively) and again seem to characteristically decrease to the E-SE. Facies proportions are marked by large presence of muclast-rich amalgamated sandstone facies (FA1) at the western and central parts of the outcrop, while at eastern parts there is a transition to channel-margin and proximal overbank facies (FA5 and FA6, Fig. 11). In the north, median sandstone thickness and its variance also show large values (especially between logs 16 and 27, Fig. 13), diminishing very rapidly towards the E-SE to values close to zero after log 27. Grain size seems to have a coarsening trend (from fine-medium to medium-coarse sand) moving from western to more eastern positions, again dropping rapidly to very fine-grained and silty towards the ESE margin. NG as well as AR and MHTP seem to all have characteristically elevated values between logs 12 and 27, with a slight decrease moving to the northwestern part (logs 11 to 3D, Fig. 13) and a significant drop in all values to the ESE (after log 27, Fig. 13). A similar trend is also observed for FA proportions, with dominance of thick-bedded, mudclast-rich amalgamated facies (FA1) between logs 12 and 27, abundance of channel-margin deposits (FA5), and dominance of overbank deposits to the ESE margin and a gradual passage to sandy channel-fill heterolithics (FA3) towards the northwestern outcrops (logs 11 to 3D, Fig. 13).

Unit 3: The unit is generally thicker than the underlying previous units ranging in thickness from around 3 up to 9 m. At more proximal positions to the south is characterized by median thicknesses of sandstone beds ranging between 10 and 25 cm across a NW-SE strike orientation, while median mudstone thicknesses are very low and close to zero. Median basal grain sizes of sandstones range from medium to coarse sand across the transect of the Southwest Outcrop, with slightly coarser values towards the E-SE (Fig. 14). Proximal NG values are extremely large (close to 100%) across the Southwest Outcrop transect, also accompanied by elevated AR and MHTP values ranging from 55 to 85% and from 5 to 30% respectively (Fig. 14). Proportions of facies associations of Unit 3 at the Southwest Outcrop are dominated by trough cross-stratified and mudclast-rich amalgamated sandstones (FA1 and FA2), while channel-margin deposits (FA5) appear at the SE margin of the proximal outcrop. In the north, the unit exhibits a gradual increase in median sandstone thickness and variation (accompanied by a concurrent decrease in mudstone thickness) moving from NW to SE positions (Fig. 15). The latter NW-to-SE-increasing trend is also observed for basal and mean grain size, which is characterized by significant content of coarse sand at the outcrops of the southeastern margin (logs 28-31). Net-to-gross, as well as AR and MHTP values, also increase from NW towards the SE margin of the outcrop, with some isolated higher values in the northwestern part (logs 3C, 3D). Proportions of facies associations reveal the main presence of mudclast-rich and trough cross-stratified channel-fill sandstones (FA1 and FA2) to the SE part of the North Outcrop and gradual dominance of both sandy and muddy channel-fill heterolithics (FA3 and FA4) at the central and northwestern part (Fig. 15).

Heterogeneity Trends for Architectural Elements ---

Lateral Accretion Packages (LAPs): Laterally accreting deposits of channelized-facies associations constituting large parts of Units 1 and 3 were interpreted as lateral-accretion packages (LAPs, *sensu* Abreu et al. 2003) and are characterized by variability in abundance of both heterolithic and sandstone-dominated facies associations (Fig. 16) as well as in values of net-to-gross and amalgamation ratio (Table 4). In general, two types of LAPs were distinguished based on fieldwork observations and statistical analysis of heterogeneity metrics: i) amalgamated and ii) semi-amalgamated LAPs, which resemble the traction dominated or amalgamated and suspension-dominated or semi-amalgamated types of LAPs originally proposed by Abreu et al. (2003).

Amalgamated LAPs: These laterally accreting channel fills are particularly exposed along the Southwest Outcrop and constitute the bulk of Units 2 and 3 exposures at the upstream part of the complex. Mean sandstone and mudstone thicknesses range around 19 and 6 cm respectively, while mean basal grain size is coarse sand. High (> 90%) values of net-to-gross and amalgamation ratio as well as larger abundances of mudclast-rich horizons (Table 4; Fig. 17) highlight the amalgamated, more proximal character of these LAPs. Mean heterogeneity metrics for individual Units (Table 6) also validate the latter, showing higher amalgamation ratios (of more than 50%) for LAPs of Units 2 and 3 at upstream outcrop localities. Highly variable proportions of cross-stratified (FA2), as well as thick-bedded mudclast-rich (FA1) sandstones are the two most dominant facies encountered (Table 5, Fig. 16), with minor abundances of the channel-margin facies association (FA5). The distribution of (log-transformed) bed thickness for mudstone and sandstone beds seems to be highly variable, and multimodal in the case of mudstone beds (Fig. 18A, B).

Semi-Amalgamated LAPs: Laterally accreting channel fills of less amalgamated nature are particularly abundant at North Outcrop localities forming a large part of Units 1 and 3 sediments. Also, this type of LAPs also forms Unit 1 deposits at upstream localities of Southwest Outcrop characterized by lower amalgamation ratios of less than 50% (Table 4). For Unit 3 LAPs, there are also lower amalgamation ratios observed for downstream localities of the North Outcrop in relation to the southern upstream localities (Table 6). Medium sand is the most abundant basal grain-size class, while mean sandstone and mudstone thickness is around 17 and 7 cm respectively. Values of net-to-gross and amalgamation ratio are generally lower than those observed for more amalgamated LAPs deposits, ranging around 80% and 40% respectively. There are also lower abundances of mudclast-rich horizons. These deposits are composed mainly of sandy heterolithic (FA3) and trough cross-stratified sand-rich (FA2) channel-fill facies associations which exhibit variable proportions (Fig. 16) with an additional contribution of muddy heterolithic (FA4) and mudclast-rich amalgamated sandstone facies associations (FA1). Bed-thickness distribution for this type of LAPs is characterized by two rather distinct, "bell-like" (normally distributed) populations both for Unit 1 and Unit 3 (downstream) LAPs, indicating the possible presence of log-normal thickness distributions (Fig. 18A, C).

Outer-Bank Bars: This bar-type element characterizes Unit 2 exposures across North Outcrop localities and is typified by thicker-bedded sandstones with a mean thickness of 22 cm and large thickness variability. Muddy layers are less abundant, having a mean thickness of 14 cm (Table 4).

Basal grain size ranges within medium-sized-sand values. This element exhibits high net-to-gross values (averaging around 70%), while mudclast-rich horizons are abundant, and amalgamation ratios average around 35% also showing large variation (Fig. 17). Mudclast-rich channel-fill sandstones (FA1) dominate (Fig. 16) with additional abundances of trough cross-stratified sandstones (FA2) and heterolithic channel-fills. This architectural element exhibits a complex multimodal bed thickness distribution of mudstone thickness, while sandstone thickness is more uniformly distributed and variable (Fig. 18B).

Inner- to Outer-Bank Transition Bars: These deposits are composed of non-amalgamated bar-like sediments showing thin-bedded laterally accreting bedsets intercalated with heterolithic sediments. They are observed mainly at North Outcrop localities directly adjacent to LAPs and were interpreted as inner- to outer-bank transition bars (*sensu* Janocko et al. 2013b), reflecting downstream deposition in relation to a large-scale laterally accreting bar represented by LAPs of Unit 3. Mean sandstone and mudstone thickness range from 10 to 12 cm respectively, and sandstone beds exhibit a mean basal grain size of fine sand (Table 4). Net-to-gross and amalgamation ratios have lower mean values (around 50 and 7% respectively, Table 4), while there are no significant abundances of mud intraclasts. Muddy and sandy heterolithic channel-fill facies associations (FA3 and FA4) constitute the bulk of these deposits, exhibiting variation (Fig. 16) with a minor contribution of cross-stratified sandstones (FA2). The distribution of bed thickness for both mudstone and sandstone beds seems to be highly variable and very similar (Fig. 18A).

Levees and/or Overbank: Heterolithic, nonchannelized facies associations adjacent to observed channel-fill deposits were interpreted as overbank sediments. They can be observed at the eastern margins of the North, Southwest, and Southeast Outcrops at both upstream and downstream localities. They are composed mainly of muddy overbank FAs (FA6 and FA7) (Table 5, Fig. 16). Mean sandstone thickness is generally low (around 5 cm), and mudstone thicknesses range close to a mean value of 25 cm. Basal grain size of beds is usually fine sand. Observed net-to-gross is generally very low (around 20%) while amalgamation ratios and mudclast-horizon thickness percentages are negligible (Table 4).

DISCUSSION

Heterogeneity of Stratigraphic Units

The observed larger-scale heterogeneity metrics for the whole stratigraphic units clearly exhibit a decreasing trend from upstream to downstream localities. The latter observation implies a general decrease in net-to-gross, amalgamation ratio and mud-intraclast abundance across a downstream distance of around 500 m (Fig. 1, Tables 3, 4). The rate of downstream decrease varies depending on the unit: Unit 1 exhibits a negligible decrease in net-to-gross and a decrease of around 50-60% in amalgamation and mud-intraclast abundance. Units 2 and 3 show a slight decrease in net-to-gross, a 50-60% decrease in amalgamation ratio, and an almost 100% decrease in mud-intraclast abundance. The overlying Unit 4 is characterized by the larger downstream differences, reaching values of more than 100%, implying a significant change in downstream evolution at the later stages of Complex 5 evolution. Facies-thickness proportions (Fig. 9) also show the dominance of heterolithic facies (FA3 and FA4) in Units 1 and 3. However, the higher occurrence of more sandstone-dominated facies (FA1, FA2, and FA5) in upstream southern localities is evident for these latter Units, especially for upper Unit 3 deposits (Figs. 11, 14). Unit 2 is dominated mainly by amalgamated sandstone facies (FA1 and FA2), which are finer grained at downstream northern localities (Figs. 11B, 13B). The overlying Unit 4 is particularly composed of heterolithics (FA3 and FA4) and large abundances of overbank facies (FA6).

Regarding heterogeneity across units, there are also some interesting findings: The lower Units 1 and 2 show an abrupt transition from sand-dominated to overbank FAs of very low net-to-gross towards the east-southeast both in upstream and downstream localities (Figs. 11C, 12C). The latter was interpreted as a transition from a channelized to a levee setting, probably situated at the outer bank of a left-turning (towards W-SW) channel bend (Marini et al., this volume). While Unit 1 seems to be composed mainly of trough cross-stratified channel-fill (FA2) and sandy heterolithic facies (FA3) of small-scale laterally accreting channelized deposits at both upstream and downstream localities (Figs. 11, 12), Unit 2 shows a different heterogeneity trend across its deposits. At the southern upstream areas (localities 60-67), Unit 2 is significantly affected by erosion, but it is composed mainly of high net-to-gross, amalgamated, laterally accreted bedsets of limited lateral extent (Fig. 11). At the downstream North Outcrop, Unit 2 is characterized by more laterally extensive, finer-grained but nevertheless still amalgamated beds, with the co-occurrence of heterolithics in their upper parts at more downstream western localities (Fig. 13). The later downstream evolution of the unit was defined as the transition from inner-bank laterally accreting deposits (at upstream localities) to finer-grained, bar-like deposits of significant lateral extent (which can even reach 500 m) probably deposited as outer-bank bars (*sensu* Nakajima et al. 2009; Fig. 7). At higher stratigraphic levels, Unit 3 shows a more peculiar character across it, with Southwest Outcrop (upstream) deposits being more coarse-grained and dominated by amalgamated facies (Figs. 14, 15). In contrast, North Outcrop (downstream) deposits of the Unit are generally more complex, being more amalgamated at the southeastern part (Fig. 15, localities 27-33 changing towards more western localities to finer-grained, heterolithic deposits (Fig. 15, localities 8-25). The later upstream and downstream trends across Unit 3 were interpreted to reflect deposition of laterally accreting channel deposits across the inner bank of a large-scale channel bend which evolved stratigraphically above channelized, outer-bank and levee deposits of Units 1 and 2. At upstream areas the more amalgamated and coarse character of Unit 3 probably reflects the existence of amalgamated, traction-dominated LAPs deposited at the upstream part of the inner bank (Abreu et al. 2003), while the less amalgamated, finer-grained character of the Unit at downstream eastern areas (Fig. 15, localities 27-33) probably reflects the deposition of less amalgamated, suspension-dominated LAPs (Abreu et al. 2003) at the more distal part of the inner bank (Fig. 7). Adjacent heterolithic deposits with abundance of amalgamated facies (Fig. 15, localities 8-25) are possibly inner- to outer-bank transition bar deposits (*sensu* Janocko et al. 2013b), reflecting the downstream transition of the inner-bank LAPs to less amalgamated deposits. Heterolithic bar-like sediments were also observed at more downstream western localities across Unit 3 (localities 3A-3C, Fig. 15), and could represent the marginal part of outer-bank bars deposited at the adjacent outer-bank area downflow.

The overlying Unit 4 exhibits a highly variable heterogeneity pattern, affected by scarcity of exposures (especially at its upstream part), which is typified by the existence of a large-scale erosional surface at its base and also by the occurrence of thin-bedded, amalgamated sandstone facies towards the southeastern part of the North Outcrop (localities 35-39), highlighting a major reorganization of the final depositional stages of the channel complex towards the east-southeast (Fig. 7; see also Marini et al., this volume).

Heterogeneity of Architectural Elements

Analysis of mean heterogeneity metrics for observed architectural elements as defined by Marini et al., this volume (Tables 4-6) confirms the existence of two types of LAPs within studied deposits of Tachrift Complex 5: i) a first type characterized by elevated values of net-to-gross (> 90%) and amalgamation ratio (> 50%), observed mainly at southern (upstream) localities of Units 2 and 3 and ii) a second type typified by lower net-to-gross (~ 80%) and amalgamation ratio (< 50%) values, which constitutes the bulk of Unit 1 deposits and can also be observed at the northern (downstream) exposures of Unit 3. The latter observation resembles previous proposals regarding variability in the degree of amalgamation of laterally accreting deposits of sinuous channels originally made by Abreu et al. (2003). Those authors observed three main types of LAPs, based also on mud-intraclast occurrence and on the spatial distribution of massive sandstones and muddy turbidites: i) amalgamated, ii) semi-amalgamated, and iii) non-amalgamated LAPs. Amalgamated LAPs *sensu* Abreu et al. (2003) are typified by amalgamated, thick sandstone beds accreting at the margins of sand-rich channels and are also characterized by high net-to-gross. Semi-amalgamated LAPs are commonly associated with high-sinuosity channels and could be characterized either by upward-thinning packages of amalgamated, thick-bedded, traction-dominated sandstones passing to thin-bedded sands at the top, or by semi-amalgamated massive sandstones interbedded with low-concentration turbidites associated with small-scale sinuous channels (Abreu et al. 2003).

Based on the above, the two types of LAPs encountered in the Tachrift Channel Complex 5 were classified as amalgamated and semi-amalgamated LAPs *sensu* Abreu et al. (2003), the former associated with thick-bedded, amalgamated deposits of Units 2 and 3 at upstream localities and the latter associated with small-scale sinuous channels of Unit 1 and downstream marginal parts of Unit 3. The heterogeneity of these LAPs is highly variable, since even amalgamated LAPs of upstream localities which exhibit large net-to-gross do not seem laterally continuous for more than 300-400 m in an east-to-west direction (perpendicular to paleoflow) and are passing to more heterolithic, less amalgamated LAPs after a downstream distance of around 500 m. Amalgamated LAPs also show a large variation of thickness, with Unit 2 LAPs (which were affected by erosion) exhibiting smaller thicknesses (of no more than 3 m) and large-scale LAPS of Unit 3 reaching a maximum thickness of 10 m at upstream areas. Outer-bank bar deposits of Unit 2 at the downstream North Outcrop (Fig. 13) are characterized by amalgamated sandstones (mainly facies associations FA1 and FA2) of good lateral extent (more than 500 m) exhibiting stable heterogeneity metrics (net-to-gross, facies proportions etc.) for more than 500 m in a strike-oriented east-to-west direction perpendicular to paleoflow (Fig. 13). Inner-to-outer-bank transition bar deposits of Unit 3 at North Outcrop (localities 8-25) are also typified by a large variation in heterogeneity expressed by highly variable mudstone thicknesses and dominance of sandy (FA3) and muddy (FA4) heterolithic FAs (Tables 5-6, Fig. 15). Levee and overbank sediments observed mainly at the eastern margins of Complex 5 are characterized by stable heterogeneity metrics typified by very low values of net-to-gross and amalgamation ratio and the dominance of proximal and distal overbank facies associations (FA6 and FA7).

Heterogeneity Trends Across a Large-Scale Channel Bend

Based on observed architectural elements and the characteristics of their heterogeneity metrics, a general quantitative framework can be established regarding expected values and ranges of some basic heterogeneity parameters across a depositional setting reflecting deposition along different stages of a large-scale channel bend (Fig. 19). Initial establishment of a left-turning bend by small-scale sinuous channels is typified by the deposition of semi-amalgamated LAPs and their adjacent levees (Unit 1) characterized by facies variation (occurrence of both amalgamated and heterolithic facies), net-to-gross around 75%, amalgamation ratio of < 50%, and distinct, normal-like bed-thickness distributions of sand and mud (Fig. 19A). Increasing sediment input during later stratigraphic stages (Unit 2) is expressed by deposition of amalgamated LAPs at the proximal part of the bend characterized by dominance of amalgamated facies, lack of heterolithics, very high net-to-gross (> 90%), and amalgamation ratios of more than 50% (Fig. 19B). At more distal localities, deposition of bar-like sediments occurs at the outer bank of the bend, characterized by dominance of amalgamated facies, high net-to-gross, amalgamation ratios of less than 50%, abundance of mud intraclasts, and occurrence of distinct, variable, and complex thickness distributions for sandstone and mudstone beds (Fig. 19B). Continuous evolution of the bend leads to the formation of large-scale LAPs (Unit 3), the upstream and downstream parts of which share similar heterogeneity characteristics with previously observed amalgamated and semi-amalgamated LAPs respectively (Fig. 19C). In the downstream area of the bend at this stage, transitional inner- to outer-bar deposits are also developing, characterized by dominance of heterolithic facies, low values of net-to-gross and amalgamation ratio, and occurrence of similar, normal-like bed thickness distributions for sand and mud layers (Fig. 19C).

CONCLUSIONS

Quantification of sedimentary heterogeneity based on data from fifty logs across the late Tortonian Tachrift Complex 5 resulted in the following findings:

- Deposits of the studied submarine-channel complex are stratigraphically organized in four main stratigraphic units which range from three to ten meters in thickness and reflect stages of channel evolution across a left-turning, large-scale channel bend.
- A range of sedimentary facies comprising different types of amalgamated sandstones, heterolithic and mud-rich sediments were recognized and grouped in channel-fill and overbank facies associations. These associations characterize four main architectural elements: lateral-accretion packages (LAPs), outer-bank bars, inner- to outer-bank transition bars, and levee and/or overbank sediments, each one demonstrating different facies proportions due to sedimentation in different depositional settings across the channel bend.
- Large-scale heterogeneity trends in stratigraphic units indicate a general decrease in net-to-gross, amalgamation ratio, and mud-intraclast abundance across a downflow distance of around 500 m across the bend. The rate of decrease varies depending on the stratigraphic unit.
- Smaller-scale heterogeneity trends in architectural elements reveal the existence of two main types of LAPs, amalgamated and semi-amalgamated ones, characterized by different values of facies proportions, net-to-gross and amalgamation ratio (AR). An observable downstream

change from amalgamated (AR > 50%) to less amalgamated (AR < 50%) LAPs is interpreted as a result of deposition in different positions across the bend's apex, with amalgamated LAPs occurring mainly at upstream apex localities.

- Observed LAP elements of Unit 3 seem to pass laterally into non-amalgamated (AR < 10%), heterolithic, laterally accreted deposits with muddy intervals characterized by high thickness variability, interpreted as transition bars between the inner and the outer bank of the apex. Also, laterally continuous, amalgamated sandstone facies of Unit 2 at downstream localities, sandwiched between LAP elements of Units 1 and 3, are typified by high net-to-gross (> 90%), higher abundances of mud intraclasts, and large variability of sandstone thickness and are interpreted to reflect an outer-bank bar element. Both elements are recorded for the first time at outcrop.
- A range of statistical characteristics of basic heterogeneity metrics (facies proportion, sandstone and mudstone thickness distribution, net-to-gross, amalgamation ratio) for each architectural element encountered is proposed, which quantitatively describe the degree of sedimentary heterogeneity across the documented large-scale slope-channel bend. Documentation of key architectural and facies-heterogeneity patterns can act as analog data to inform the simplification and upscaling required to reduce uncertainty for reservoir modeling of similar slope-channel-fills.

ACKNOWLEDGMENTS

The authors would like to thank the Turbidite Research Group (University of Leeds) for continuous support of research activities at the Taza-Guercif Basin area, with funding provided by AkerBP, CNOOC, ConocoPhillips, Harbour Energy, Murphy Oil, OMV, PetroChina, and OXY. Editorial handling by George Postma, Peter Burgess, Dustin Sweet, and John Southard, as well as constructive comments and suggestions by journal reviewers Zane Jobe and Bradford Prather, significantly improved an initial version of the manuscript and are thankfully acknowledged. Many thanks to Prof. Hassan Tabyaoui (Sidi Mohamed Ben Abdellah University, Fez) for logistical support during fieldwork. The authors are grateful to Hachimi family (Ait El Baji) for their warm hospitality and invaluable help during the stay at Morocco.

REFERENCES

Abreu, V., Sullivan, M., Pirmez, C., and Mohrig, D., 2003, Lateral accretion packages (LAPs): an important reservoir element in deep water sinuous channels: Marine and Petroleum Geology: v. 20, p. 631-648.

Arnott, R.W.C., 2007, Stratal architecture and origin of lateral accretion deposits (LADs) and conterminuous inner-bank levee deposits in a base-of-slope sinuous channel, lower Isaac Formation (Neoproterozoic), East-Central British Columbia, Canada: Marine and Petroleum Geology, v. 24, p. 515-528.

Arnott, R.W.C., Tilston, M., Fraino, P., Navarro, L., Dumouchel, G., and Miklovich, N., 2021, Laterally accreting sinuous channels and their deposits: The Goldilocks of deep-water slope systems: Journal of Sedimentary Research, v. 91, p. 451-463.

Babonneau, N., Savoye, B., Cremer, M., and Bez, M., 2004, Multiple terraces within the deep incised Zaire Valley (ZaiAngo Project): are they confined levees? *in* Lomas, S.A., and Joseph, P., eds., Confined Turbidite Systems: Geological Society of London, Special Publication 222, p. 91-114.

Babonneau, N., Savoye, B., Cremer, M., and Bez, M., 2010, Sedimentary architecture in meanders of a submarine channel: Detailed study of the Present Congo Turbidite Channel (Zaiango Project): Journal of Sedimentary Research, v. 80, p. 852-866.

Bell, D., Hodgson, D.M., Pontén, A.S.M., Hansen, L.A.S., Flint, S.S., and Kane, I.A., 2020, Stratigraphic hierarchy and three-dimensional evolution of an exhumed submarine slope channel system: Sedimentology, v. 67, p. 3259-3289.

Benzaquen, M., 1965, Etude stratigraphique préliminaire des formations du bassin de Guercif: Direct. Mines et Géologie, Service de la Cartographie Géologique, Bureau d'études des bassins Sédimentaires, 73 p.

Bernini, M., Boccaletti, M., El Mokhtari, J., Gelati, R., Moratti, G., and Papani, G., 1994, Geologic-structural Map of the Taza-Guercif Neogene basin (North-eastern Morocco): Società Elaborazioni Cartografiche, Firenze, scale 1:50,000.

Bernini, M., Boccaletti, M., Gelati, R., Moratti, G., Papani, G., and Mokhtari, J.E., 1999, Tectonics and sedimentation in the Taza-Guercif Basin, Northern Morocco: Implications for the Neogene Evolution of the Rif-Middle Atlas Orogenic system: Journal of Petroleum Geology, v. 22, p. 115-128.

Bernini, M., Boccaletti, M., Moratti, G., and Papani, G., 2000, Structural development of the Taza-Guercif Basin as a constraint for the Middle Atlas Shear Zone tectonic evolution: Marine and Petroleum Geology, v. 17, p. 391-408.

Bouma, A.H., 1962, Sedimentology of Some Flysch Deposits; A Graphic Approach to Facies Interpretation: Elsevier, Amsterdam, 168 p.

Bozetti, G., Kneller, B., Cronin, B.T., Li, P., McArthur, A. and Xu, J., 2023, Lateral and temporal variations of a multi-phase coarse-grained submarine slope channel system, upper Cretaceous Cerro Toro Formation, southern Chile: Journal of Sedimentary Research, v. 93, p. 161-186.

Bruhn, C.H.L., and Walker, R.G., 1997, Internal architecture and sedimentary evolution of coarse-grained, turbidite channel-levee complexes, early Eocene Regência canyon, Espirito Santo Basin, Brazil: Sedimentology, v. 44, p. 17-46.

Capella, W., Hernandez-Molina, F.J., Flecker, R., Hilgen, F.J., Hssain, M., Kouwenhoven, T.J., van Oorschot, M., Sierro, F.J., Stow, D.A.V., Trabucho-Alexandre, J., Tulbure, M.A., de Weger, W., Yousfi, M.Z., and Krijgsman, W., 2017, Sandy contourite drift in the late Miocene Rifian Corridor (Morocco): Reconstruction of depositional environments in a foreland-basin seaway: Sedimentary Geology, v. 355, p. 31-57.

Capella, W., Barhoun, N., Flecker, R., Hilgen, F.J., Kouwenhoven, T., Matenco, L.C., Sierro, F.J., Tulbure, M.A., Yousfi, M.Z., and Krijgsman, W., 2018, Palaeogeographic evolution of the late Miocene Rifian Corridor (Morocco): reconstructions from surface and subsurface data: Earth-Science Reviews, v. 180, p. 37-59.

Capella, W., Flecker, R., Hernández-Molina, F.J., Simon, D., Meijer, P.T., Rogerson, M., Sierro, F.J., and Krijgsman, W., 2019, Mediterranean isolation preconditioning the Earth System for late Miocene climate cooling: Scientific Reports, v. 9, no.3795.

Clark, J.D., and Pickering, K.T., 1996, Architectural elements and growth patterns of submarine channels: application to hydrocarbon exploration: American Association of Petroleum Geologists, Bulletin, v. 80, p. 194-221.

Clark, J.D., Kenyon, N.H., and Pickering, K., 1992, Quantitative analysis of the geometry of submarine channels: implications for the classification of submarine fans: Geology, v. 20, p. 633-636.

Crisóstomo-Figueroa, A., Dorrell, R.M., Amy, L., McArthur, A.D. and McCaffrey, W.D., 2024, Modeling the Tilt of Bend-Traversing Turbidity Currents: Implications for Sinuous Submarine Channel Development: Journal of Geophysical Research: Oceans, v. 129, no. e2023JC020131.

Deptuck, M.E., and Sylvester, Z., 2018, Submarine Fans and Their Channels, Levees, and Lobes, *in* Micallef, A., Krastel, S., and Savini, A., eds., Submarine Geomorphology: Springer, p. 273-299.Deptuck, M.E., Steffens, G.S., Barton, M., and Pirmez, C., 2003, Architecture and evolution of upper fan channel-belts on the Niger Delta slope and in the Arabian Sea: Marine and Petroleum Geology, v. 20, p. 649-676.

Deptuck, M.E., Sylvester, Z., Pirmez, C., and O'Byrne, C., 2007, Migration-aggradation history and 3D seismic geomorphology of submarine channels in the Pleistocene Benin-major Canyon, western Niger Delta slope: Marine and Petroleum Geology, v. 24, p. 406-433.

Dykstra, M., and Kneller, B., 2009, Lateral accretion in a deep-marine channel complex: implications for channellized flow processes in turbidity currents: Sedimentology, v. 56, p. 1411-1432.

Elliott, T., 2000, Depositional Architecture of a Sand-Rich, Channelized Turbidite System: The Upper Carboniferous Ross Sandstone Formation, Western Ireland, *in* Weimer, P., ed., Deep-Water Reservoirs of the World: Gulf Coast Section Society for Sedimentary Geology Publications, Texas, Gulf Coast Section Society for Sedimentary Geology Foundation Annual Bob F. Perkins Research Conference, Proceedings, v. 20, p. 342-373.

Felletti, F., Marini, M., El Kati, I., and Tabyaoui, H., 2020, The Tachrift channel-levée turbidite complexes (Tortonian) of the Taza-Guercif basin (South Rifian Corridor, NE Morocco): Journal of Maps, v. 16, p. 902-917.

Felletti, F., Pantopoulos, G., Zuffetti, C., Reguzzi, S., Invernizzi, D., Bellin, N., Marini, M., El Kati, I., Savi, E., Tabyaoui, H., and McArthur, A., 2023, The Tachrift Project: sedimentary architecture of turbidite channel-levée deposits (Tachrift Turbidite System, Taza-Guercif Basin, Tortonian, NE Morocco): Rendiconti Online della Società Geologica Italiana, v. 59, p. 80-88.

Flecker, R., Krijgsman, W., Capella, W., de Castro Martins, C., Dmitrieva, E., Mayser, J.P., Marzocchi, A., Modestou, S., Ochoa, D., Simon, D., Tulbure, M., van den Berg, B., van der Schee, M., de Lange, G., Ellam, R., Govers, R., Gutjahr, M., Hilgen, F., Kouwenhoven, T., Lofi, J., Meijer, P., Sierro, F.J., Bachiri, N., Barhoun, N., Alami, A.C., Chacon, B., Flores, J.A., Gregory, J., Howard, J., Lunt, D., Ochoa, M., Pancost, R., Vincent, S., and Yousfi, M.Z., 2015, Evolution of the Late Miocene Mediterranean-Atlantic gateways and their impact on regional and global environmental change: Earth-Science Reviews, v. 150, p. 365-392.

Fryer, R.C., and Jobe, Z.R., 2019, Quantification of the bed-scale architecture of submarine depositional environments: The Depositional Record, v. 5, p. 192-211.

Funk, J.E., Slatt, R.M., and Pyles, D.R., 2012, Quantification of static connectivity between deep-water channels and stratigraphically adjacent architectural elements using outcrop analogs: American Association of Petroleum Geologists, Bulletin, v. 96, p. 277-300.

Gamberi, F., Rovere, M., Dykstra, M., Kane, I.A., and Kneller, B.C., 2013, Integrating modern seafloor and outcrop data in the analysis of slope channel architecture and fill: Marine and Petroleum Geology, v. 41, p. 83-103.

Gardner, M.H., Borer, J.M., Melick, J.J., Mavilla, N., Dechesne, M., and Wagerle, R.N., 2003, Stratigraphic process-response model for submarine channels and related features from studies of Permian Brushy Canyon outcrops, West Texas: Marine and Petroleum Geology, v. 20, p. 757-787.

Gelati, R., Moratti, G. and Papani, G., 2000, The Late Cenozoic sedimentary succession of the Taza-Guercif Basin, South Rifian Corridor, Morocco: Marine and Petroleum Geology, v. 17, p. 373-390.

Hafid, M., Zizi, M., Bally, A.W., and Salem, A.A., 2006, Structural styles of the western onshore and offshore termination of the High Atlas, Morocco: Comptes Rendus Geoscience, v. 338, p. 50-64.

Hansen, L.A., Callow, R.H., Kane, I.A., Gamberi, F., Rovere, M., Cronin, B.T., and Kneller, B.C., 2015, Genesis and character of thin-bedded turbidites associated with submarine channels: Marine and Petroleum Geology, v. 67, p. 852-879.

Hansen, L., Callow, R., Kane, I., and Kneller, B., 2017, Differentiating submarine channel-related thin-bedded turbidite facies: Outcrop examples from the Rosario Formation, Mexico: Sedimentary Geology, v. 358, p. 19-34.

Hubbard, S.M., Covault, J.A., Fildani, A., and Romans, B.W., 2014, Sediment transfer and deposition in slope channels: Deciphering the record of enigmatic deep-sea processes from outcrop: Geological Society of America, Bulletin, v. 126, p. 857-871.

Hubbard, S.M., Jobe, Z.R., Romans, B.W., Covault, J.A., Sylvester, Z., and Fildani, A., 2020, The stratigraphic evolution of a submarine channel: Linking seafloor dynamics to depositional products: Journal of Sedimentary Research, v. 90, p. 673-686.

Janocko, M., Nemec, W., Henriksen, S., and Warchoł, M., 2013a, The diversity of deep-water sinuous channel belts and slope valley-fill complexes: Marine and Petroleum Geology, v. 41, p. 7-34.

Janocko, M., Cartigny, M.B.J., Nemec, W., and Hansen, E.W.M., 2013b, Turbidity current hydraulics and sediment deposition in erodible sinuous channels: laboratory experiments and numerical simulations: Marine and Petroleum Geology, v. 41, p. 222-249.

Jobe, Z.R., Sylvester, Z., Parker, A.O., Howes, N., Slowey, N., and Pirmez, C., 2015, Rapid adjustment of submarine channel architecture to changes in sediment supply: Journal of Sedimentary Research, v. 85, p. 729-753.

Jobe, Z.R., Howes, N.C., and Auchter, N.C., 2016, Comparing submarine and fluvial channel kinematics: Implications for stratigraphic architecture: Geology, v. 44, p. 931-934.

Jobe, Z.R, Howes, N., Martin, J., Meyer, R., Coutts, D., Hou, P., Stright, L., and Laugier, F., 2021, Sedimentary Graphic Logs: A Template for Description and a Toolkit for Digitalization: The Sedimentary Record, v. 19, p. 15-29.

Kane, I.A., and Clare, M.A., 2019, Dispersion, accumulation, and the ultimate fate of microplastics in deep-marine environments: A review and future directions: Frontiers in Earth Science, v. 7, art. no. 80.

Kane, I.A., and Hodgson, D.M., 2011, Sedimentological criteria to differentiate submarine channel levee subenvironments: exhumed examples from the Rosario Fm. (Upper Cretaceous) of Baja California, Mexico, and the Fort Brown Fm. (Permian), Karoo basin, S. Africa: Marine and Petroleum Geology, v. 28, p. 807-823.

Kane, I.A., Kneller, B.C., Dykstra, M., Kassem, A., and McCaffrey, W.D., 2007, Anatomy of a submarine channel-levee: An example from Upper Cretaceous slope sediments, Rosario Formation, Baja California, Mexico: Marine and Petroleum Geology, v. 24, p. 540-563.

Kane, I.A., Dykstra, M.L., Kneller, B.C., Tremblay, S., and McCaffrey, W.D., 2009, Architecture of a coarse-grained channel-levée system: The Rosario Formation, Baja California, Mexico: Sedimentology, v. 56, p. 2207-2234.

Khan, Z.A., and Arnott, R.W.C., 2011, Stratal attributes and evolution of asymmetric inner-and outer-bend levee deposits associated with an ancient deep-water channel-levee complex within the Isaac Formation, southern Canada: Marine and Petroleum Geology, v. 28, p. 824-842.

Kneller, B., Bozetti, G., Callow, R., Dykstra, M., Hansen, L., Kane, I., Li, P., McArthur, A., Catharina, A.S., Dos Santos, T., and Thompson, P., 2020, Architecture, process, and environmental diversity in a late Cretaceous slope channel system: Journal of Sedimentary Research, v. 90, p. 1-26.

Kolla, V., 2007, A review of sinuous channel avulsion patterns in some major deep-sea fans and factors controlling them: Marine and Petroleum Geology, v. 24, p. 450-469.

Kolla, V., Bourges, P., Urruty, J.M., and Safa, P., 2001, Evolution of deep-water Tertiary sinuous channels offshore Angola (west Africa) and implications for reservoir architecture: American Association of Petroleum Geologists, Bulletin, v. 85, p. 1373-1405.

Kolla, V., Posamentier, H.W., and Wood, L.J., 2007, Deep-water and fluvial sinuous channels-Characteristics, similarities and dissimilarities, and modes of formation: Marine and Petroleum Geology, v. 24, p. 388-405.

Krijgsman, W., and Langereis, C.G., 2000, Magnetostratigraphy of the Zobzit and Koudiat Zarga sections (Taza-Guercif basin, Morocco): Implications for the evolution of the Rifian Corridor: Marine and Petroleum Geology, v. 17, p. 359-371.

Krijgsman, W., Langereis, C.G., Zachariasse, W.J., Boccaletti, M., Moratti, G., Gelati, R., Iaccarino, S., Papani, G., and Villa, G., 1999, Late Neogene evolution of the Taza–Guercif Basin (Rifian Corridor, Morocco) and implications for the Messinian salinity crisis: Marine Geology, v. 153, p. 147-160.

Kus, K.B., Jobe, Z.R., Laugier, F., Walker, W., and Sullivan, M., 2022, Quantifying the lateral heterogeneity of distal submarine lobe deposits, Point Loma Formation, California: Implications for subsurface lateral facies prediction: The Depositional Record, v. 8, p. 472-501.

Li, P., Kneller, B.C., Hansen, L., and Kane, I.A., 2016, The classical turbidite outcrop at San Clemente, California revisited: An example of sandy submarine channels with asymmetric facies architecture: Sedimentary Geology, v. 346, p. 1-16.

Li, P., Kneller, B., Thompson, P., Bozetti, G., and dos Santos, T., 2018, Architectural and facies organisation of slope channel fills: Upper Cretaceous Rosario Formation, Baja California, Mexico: Marine and Petroleum Geology, v. 92, p. 632-649.

Lien, T., Walker, R.G., and Martinsen, O.J., 2003, Turbidites in the Upper Carboniferous Ross Formation, western Ireland: reconstruction of a channel and spillover system: Sedimentology, v. 50, p. 113-148.

Lobato, G., Postma. G., Lintern, D.G., Jacinto, R.S., and Cartigny, M.J.B., this volume, Decadal architecture and morphodynamics of modern, river-fed turbidite systems: Bute Inlet and Congo Fan: Journal of Sedimentary Research.

Lowe, D.R., 1982, Sediment gravity flows; II, Depositional models with special reference to the deposits of high-density turbidity currents: Journal of Sedimentary Petrology, v. 52, p. 279-297.

Macauley, R.V., and Hubbard, S.M., 2013, Slope channel sedimentary processes and stratigraphic stacking, Cretaceous Tres Pasos Formation slope system, Chilean Patagonia: Marine and Petroleum Geology, v. 41, p. 146-162.

Macdonald, H.A., Peakall, J., Wignall, P.B., and Best, J., 2011, Sedimentation in deep-sea lobe elements: implications for the origin of thickening-upward sequences: Journal of the Geological Society, v. 168, p. 319-332.

Maier, K.L., Fildani, A., Paull, C.K., McHargue, T.R., Graham, S.A., and Caress, D.W., 2013, Deep-sea channel evolution and stratigraphic architecture from inception to abandonment from high-resolution autonomous underwater vehicle surveys offshore central California: Sedimentology, v. 60, p. 935-960.

Marini, M., Pantopoulos, G., Invernizzi, D., Felletti, F., El Kati, I., and McArthur, A., this volume, Temporal and spatial changes in style of accretion at the bend of a sinuous turbidite slope channel (channel levee Complex 5, Tachrift System 0f NE Morocco): Journal of Sedimentary Research.

Mayall, M., and Stewart, I., 2000, The Architecture of Turbidite Slope Channels, *in* Weimer, P., ed., Deep-Water Reservoirs of the World: Gulf Coast Section Society for Sedimentary Geology

Publications, Texas, Gulf Coast Section Society for Sedimentary Geology Foundation Annual Bob F. Perkins Research Conference, Proceedings, v. 20, p. 578-586.

Mayall, M., Jones, E., and Casey, M., 2006, Turbidite channel reservoirs–key elements in facies prediction and effective development: Marine and Petroleum Geology, v. 23, p. 821-841.

McArthur, A.D., Kneller, B.C., Souza, P.A., and Kuchle, J., 2016, Characterization of deep-marine channel-levee complex architecture with palynofacies: An outcrop example from the Rosario Formation, Baja California, Mexico: Marine and Petroleum Geology, v. 73, p. 157-173.

McHargue, T., Pyrcz, M.J., Sullivan, M.D., Clark, J.D., Fildani, A., Romans, B.W., Covault, J.A., Levy, M., Posamentier, H.W., and Drinkwater, N.J., 2011, Architecture of turbidite channel systems on the continental slope: Patterns and predictions: Marine and Petroleum Geology, v. 28, p. 728-743.

Moody, J.D., Pyles, D.R., Clark, J., and Bouroullec, R., 2012, Quantitative outcrop characterization of an analog to weakly confined submarine channel systems: Morillo 1 member, Ainsa Basin, Spain: American Association of Petroleum Geologists, Bulletin, v. 96, p. 1813-1841.

Morris, E.A., Hodgson, D.M., Flint, S., Brunt, R.L., Luthi, S.M., and Kolenberg, Y., 2016, Integrating outcrop and subsurface data to assess the temporal evolution of a submarine channel-levee system: American Association of Petroleum Geologists, Bulletin, v.100, p. 1663-1691.

Mutti, E., 1992, Turbidite Sandstones: Agip / Istituto di Geologia Università di Parma, 275 p.

Mutti, E., and Normark, W. R., 1987, Comparing examples of modern and ancient turbidite systems: problems and concepts, *in* Leggett, J.K., and Zuffa, G.G., eds., Marine Clastic Sedimentology: Concepts and Case Studies: Graham and Trotman, London, p. 1-38.

Nakajima, T., and Kneller, B.C., 2013, Quantitative analysis of the geometry of submarine external levees: Sedimentology, v. 60, p. 877-910.

Nakajima, T., Peakall, J., McCaffrey, W.D., Paton, D.A., and Thompson, P.J., 2009, Outer-bank bars: a new intra-channel architectural element within sinuous submarine slope channels: Journal of Sedimentary Research, v. 79, p. 872-886.

Pantopoulos, G., Kneller, B.C., McArthur, A.D., Courivaud, S., Grings, A.E., and Kuchle, J., 2018, Turbidite bed thickness statistics of architectural elements in a deep-marine confined mini-basin setting: Examples from the Grès d'Annot Formation, SE France: Marine and Petroleum Geology, v. 95, p. 16-29.

Patacci, M., 2016, A high-precision Jacob's staff with improved spatial accuracy and laser sighting capability: Sedimentary Geology, v. 335, p. 66-69.

Peakall, J., and Sumner, E.J., 2015, Submarine channel flow processes and deposits: A process-product perspective: Geomorphology, v. 244, p. 95-120.

Peakall, J., McCaffrey, B., and Kneller, B., 2000, A process model for the evolution, morphology, and architecture of sinuous submarine channels: Journal of Sedimentary Research, v. 70, p. 434-448.

Peakall, J., Amos, K.J., Keevil, G.M., Bradbury, P.W., and Gupta, S., 2007, Flow processes and sedimentation in submarine channel bends: Marine and Petroleum Geology, v. 24, p. 470-486.

Piper, D.J.W., and Aksu, A.E., 1987, The source and origin of the 1929 grand banks turbidity current inferred from sediment budgets: Geo-Marine Letters, v. 7, p. 177-182.

Pirmez, C., and Imran, J., 2003, Reconstruction of turbidity currents in Amazon Channel: Marine and Petroleum Geology, v. 20, p. 823-849.

Prather, B.E., 2003, Controls on reservoir distribution, architecture and stratigraphic trapping in slope settings: Marine and Petroleum Geology, v. 20, p. 529-545.

Pratt, J.R., Barbeau, D.L., Jr., Izykowski, T.M., Garver, J.I., and Emran, A., 2016, Sedimentary provenance of the Taza-Guercif Basin, South Rifean Corridor, Morocco: Implications for basin emergence: Geosphere, v. 12, p. 221-236.

Pringle, J.K., Brunt, R.L., Hodgson, D.M., and Flint, S.S., 2010, Capturing stratigraphic and sedimentological complexity from submarine channel complex outcrops to digital 3D models, Karoo Basin, South Africa: Petroleum Geoscience, v. 16, p. 307-330.

Pyles, D.R., Jennette, D.C., Tomasso, M., Beaubouef, R.T., and Rossen, C., 2010, Concepts learned from a 3d outcrop of a sinuous slope channel complex: Beacon Channel Complex, Brushy Canyon Formation, West Texas, U.S.A.: Journal of Sedimentary Research, v. 80, p. 67-96.

R Core Team, 2022, R: A language and environment for statistical computing: R Foundation for Statistical Computing, Vienna, Austria. URL https://www.R-project.org/.

Reguzzi, S., Marini, M., Felletti, F., El Kati, I., Zuffetti, C., and Tabyaoui, H., 2023, Stratigraphic evolution of a spectacularly exposed turbidite channel belt from the Tachrift System (late Tortonian, north-East Morocco): Sedimentology, v. 70, p. 1075-1109.

Reimchen, A.P., Hubbard, S.M., Stright, L., and Romans, B.W., 2016, Using sea-floor morphometrics to constrain stratigraphic models of sinuous submarine channel systems: Marine and Petroleum Geology, v. 77, p. 92-115.

Romans, B.W., Hubbard, S.M. and Graham, S.A., 2009, Stratigraphic evolution of an outcropping continental slope system, Tres Pasos Formation at Cerro Divisadero, Chile: Sedimentology, v. 56, p. 737-764.

Ruffell, S.C., Talling, P.J., Baker, M.L., Pope, E.L., Heijnen, M.S., Jacinto, R.S., Cartigny, M.J.B., Simmons, S.M., Clare, M.A., Heerema, C.J., McGhee, C., Hage, S., Hasenhündl, M., and Parsons, D.R., 2024, Time-lapse surveys reveal patterns and processes of erosion by exceptionally powerful turbidity currents that flush submarine canyons: A case study of the Congo Canyon: Geomorphology, v. 463, art. no. 109350.

Sani, F., Zizi, M., and Bally, A.W., 2000, The Neogene–Quaternary evolution of the Guercif Basin (Morocco) reconstructed from seismic line interpretation: Marine and Petroleum Geology, v. 17, p. 343-357.

Schwarz, E., and Arnott, R.W.C., 2007, Anatomy and evolution of a slope channel-complex set (Neoproterozoic Isaac Formation, Windermere Supergroup, southern Canadian Cordillera): implications for reservoir characterization: Journal of Sedimentary Research, v. 77, p. 89-109.

Straub, K.M., Mohrig, D., Buttles, J., McElroy, B., and Pirmez, C., 2011, Quantifying the influence of channel sinuosity on the depositional mechanics of channelized turbidity currents: a laboratory study: Marine and Petroleum Geology, v. 28, p. 744-760.

Sylvester, Z., 2007, Turbidite bed thickness distributions: Methods and pitfalls of analysis and modelling: Sedimentology, v. 54, p. 847-870.

Sylvester, Z., and Covault, J.A., 2016, Development of cutoff-related knickpoints during early evolution of submarine channels: Geology, v. 44, p. 835-838

Sylvester, Z., Pirmez, C., and Cantelli, A., 2011, A model of submarine channel–levee evolution based on channel trajectories: implications for stratigraphic architecture: Marine and Petroleum Geology, v. 28, p. 716-727.

Talling, P.J., Wynn, R.B., Masson, D.G., Frenz, M., Cronin, B.T., Schiebel, R., Akhmetzhanov, A.M., Dallmeier-Tiessen, S., Benetti, S., Weaver, P.P.E., Georgiopoulou, A., Zühlsdorff, C., and Amy, L.A., 2007, Onset of submarine debris flow deposition far from original giant landslide: Nature, v. 450, p. 541-544.

Tek, D.E., McArthur, A.D., Poyatos-Moré, M., Colombera, L., Patacci, M., Craven, B., and McCaffrey, W.D., 2021, Relating seafloor geomorphology to subsurface architecture: How mass-transport deposits and knickpoint-zones build the stratigraphy of the deep-water Hikurangi Channel: Sedimentology, v. 68, p. 3141-3190.

Tek, D.E., McArthur, A.D., Poyatos-Moré, M., Colombera, L., Allen, C., Patacci, M., and McCaffrey, W.D., 2022, Controls on the architectural evolution of deep-water channel overbank sediment wave fields: insights from the Hikurangi Channel, offshore New Zealand: New Zealand Journal of Geology and Geophysics, v. 65, p. 141-178.

Tinterri, R., and Civa, A., 2021, Laterally accreted deposits in low efficiency turbidites associated with a structurally-induced topography (Oligocene Molare Group, Tertiary Piedmont Basin, NW Italy): Journal of Sedimentary Research, v. 91, p. 751-772.

Walker, R.G., 1975, Nested submarine-fan channels in the Capistrano Formation, San Clemente, California: Geological Society of America, Bulletin, v. 86, p. 915-924.

Weimer, P., Slatt, R.M., Dromgoole, P., Bowman, M., and Leonard, A., 2000, Developing and managing turbidite reservoirs - case histories and experiences: results of the 1998 European Association of Geoscientists and Engineers / American Association of Petroleum Geologists, research conference: American Association of Petroleum Geologists, Bulletin, v. 84, p. 453-465.

Wynn, R.B., Cronin, B.T., and Peakall, J., 2007, Sinuous deep-water channels: Genesis, geometry and architecture: Marine and Petroleum Geology, v. 24, p. 341-387.

Zuffetti, C., Felletti, F., and Marini, M., 2023, Turbidite channel-levée transitions: insights from the Tachrift system (Complex 6, Taza-Guercif Basin, NE Morocco): Rendiconti Online della Società Geologica Italiana, v. 59, p. 21-27.

CAPTIONS

Fig. 1: A) Geological sketch map of northern Morocco illustrating key structural elements and main terranes and Cenozoic basins (modified after Hafid et al. 2006). B) Schematic geological map of the Taza-Guercif basin (modified, after Bernini et al. 1994) with study area shown. C) Stratigraphy of the Zobzit section with magnetostratigraphy (left-hand side), and numbers identifying the channel-levee complexes of Felletti et al. (2020) (modified, after Krijgsman et al. 1999). D) Geological map of the Tachrift Complex 5 outcrop area, showing the three main outcrop transects studied, log localities (with numbers), main tectonic structures, and main paleoflow trend.

Fig. 2: Stratigraphic panel of Complex 5 outcrops exhibiting the main stratigraphic Units (1-4) recognized. A) North Outcrop. B) Southwest Outcrop. C) Southeast Outcrop.

Fig. 3: General aspects of stratigraphic units in both North and Southwest Outcrops: A) View of stratigraphic units between logs 17 and 20 of North Outcrop. B) Organization of stratigraphic units observed between logs 27 and 30 at North Outcrop localities. Accretion of sandy bodies in Unit 3 towards the east can be also seen (black arrow). Frameworks highlight outcrop details presented in Fig. 5. C) View of stratigraphic arrangement of units between logs 60 and 62 at Southwest Outcrop localities. Lateral shifting of sandy bodies in Unit 3 can be also seen (black arrow). Frameworks highlight outcrop details presented in Fig. 6. D) Aspects of observed stratigraphy between logs 66 and 67 at the southwestern part of the complex, in which the four stratigraphic units can be seen.

Fig 4: Log examples, sedimentological description, and interpretation of observed facies associations (FA1-FA7). Colors used for representing each FA in figures are also presented.

Fig. 5: Outcrop photos of observed facies associations at Northern Outcrop locations: A) Proximal and distal overbank deposits (FA6 and FA7) near log 28. B) Muddy heterolithic channel-fills (FA4) overlying trough cross-stratified sandstones (FA2) between logs 29 and 30. C) Sandy heterolithic channel-fill sandstones (FA3), log 28. D) Thin-bedded amalgamated channel-margin deposits of

FA5, log 27. E) Trough cross-stratified channel-fill sandstones (FA2), near log 30. F) Thick-bedded, mud clast-rich amalgamated sandstone of FA1, log 27.

Fig. 6: Outcrop photos of observed facies at Southwest Outcrop locations: A) Proximal and distal overbank sediments (FA6 and FA7) underlying channel-margin sandstones of FA5 between logs 60 and 61. B) Proximal overbank deposits (FA6) underlying channel-margin FA5 sandstones, log 60. C) Sandy heterolithic channel-fill sandstones (FA3), underlying mudclast-rich amalgamated sandstones of FA1, between logs 65 and 66. D) Thin-bedded, amalgamated, mudclast-rich channel-margin sandstones of FA5, near log 61. E) Trough cross-stratified amalgamated sandstones of FA2, top of log 61. F) Thick-bedded, mudclast-rich amalgamated sandstone of FA1, near log 64.

Table 1: Sedimentary facies recognized in the studied part of Tachrift Channel Complex 5. See also Marini et al., this volume.

Fig. 7: A)-D) Paleogeographic map exhibiting the depositional evolution of Units 1 to 4 of Tachrift Channel Complex 5, reconstructed from stratigraphic correlations and field measurements of paleoflow and lateral-accretion directions (see also Marini et al., this volume).

Table 2: Descriptive statistics of thickness and grain size for sandstone and mudstone beds across stratigraphic units of Tachrift Channel Complex 5.

Table 3: Descriptive statistics for net-to-gross (NG), amalgamation ratio (AR), and mud-clast-horizon thickness percentage (MHTP), for Southwest, Southeast (upstream), and North (downstream) Outcrops of stratigraphic Units of the Tachrift Channel Complex 5.

Fig. 8: Boxplots showing distribution of net-to-gross (NG), amalgamation ratio (AR), and mud-clast-horizon thickness percentage (MHTP) for all outcrops and individual stratigraphic units of Tachrift

Complex 5. Data for all outcrops (left), North Outcrop (center), and Southern outcrops (right): A) Unit 1, B) Unit 2, C) Unit 3, D) Unit 4.

Fig. 9: Stratigraphic panel of Complex 5 outcrops exhibiting spatial distribution of facies associations (FA1-FA7) recognized: A) North Outcrop, B) Southwest Outcrop, C) Southeast Outcrop.

Fig. 10: A) Boxplots exhibiting observed variation in facies-association thickness percentage for individual stratigraphic units. B) Pie charts of mean facies-association composition for each stratigraphic unit. Data of all outcrops are included.

Fig. 11: Examples of the observed trends of heterogeneity metrics for deposits of Unit 1 at Southwest Outcrop (left) and Unit 2 at the same outcrop (right). A) Boxplots for sandstone and mudstone thickness for each log. B) Boxplots of grain-size variation for basal and mean grain size of beds across logs. C) Facies-associations thickness proportions. D) Biplots showing net-to-gross, amalgamation ratio, and mudclast-horizon thickness percentage across Unit 1. Characteristic logs of the Unit with interpreted architectural elements are on top.

Fig. 12: Examples of the observed trends of heterogeneity metrics for deposits of Unit 1 at North Outcrop. A) Boxplots for sandstone and mudstone thickness for each log. B) Boxplots of grain-size variation for basal and mean grain size of beds across logs. C) Facies-associations thickness proportions. D) Biplots showing net-to-gross, amalgamation ratio, and mudclast-horizon thickness percentage across Unit 1. Characteristic logs of the Unit with interpreted architectural elements are on top.

Fig. 13: Examples of the observed trends of heterogeneity metrics for deposits of Unit 2 at North Outcrop. A) Boxplots for sandstone and mudstone thickness for each log. B) Boxplots of grain-size variation for basal and mean grain size of beds across logs. C) Facies-associations thickness proportions. D) Biplots showing net-to-gross, amalgamation ratio, and mudclast-horizon thickness

percentage across Unit 1. Characteristic logs of the Unit with interpreted architectural elements are on top.

Fig. 14: Examples of the observed trends of heterogeneity metrics for deposits of Unit 3 at Southwest Outcrop. A) Boxplots for sandstone and mudstone thickness for each log. B) Boxplots of grain-size variation for basal and mean grain size of beds across logs. C) Facies-associations thickness proportions. D) Biplots showing net-to-gross, amalgamation ratio, and mudclast-horizon thickness percentage across Unit 1. Characteristic logs of the Unit with interpreted architectural elements are on top.

Fig. 15: Examples of the observed trends of heterogeneity metrics for deposits of Unit 3 at North Outcrop. A) Boxplots for sandstone and mudstone thickness for each log. B) Boxplots of grain-size variation for basal and mean grain size of beds across logs. C) Facies-associations thickness proportions. D) Biplots showing net-to-gross, amalgamation ratio, and mudclast-horizon thickness percentage across Unit 1. Characteristic logs of the Unit with interpreted architectural elements are on top.

Fig. 16: Variations of facies-associations thickness proportion for each architectural element of Channel Complex 5.

Fig. 17: Variations of net-to-gross, amalgamation ratio, and mudclast-horizon thickness percentage for each architectural element of Channel Complex 5.

Fig. 18: Distributions of sandstone and mudstone bed thickness (in natural log-transformed values) for observed architectural elements across Southwest (upstream) and North (downstream) Outcrops.

Table 4: Mean values for heterogeneity metrics for architectural elements observed. Bold numbers highlight higher values characterizing specific elements.

Table 5: Mean values for facies-associations thickness proportions for architectural elements observed. Bold numbers highlight the 2 main FAs dominating in each element.

Table 6: Mean values of heterogeneity metrics for upstream and downstream Outcrops of Units 1 to 3. Abbreviations: IOBTB - Inner to Outer Bar Transition Bar, LAPs – Lateral-Accretion Packages, LV – Levee, OBB – Outer-Bank Bar.

Fig. 19: Basic statistical characteristics (illustrating facies-associations percentage, sandstone and mudstone thickness distribution, mean net-to-gross etc.) of each architectural element for Units 1-3 of Tachrift Channel Complex 5. All elements reflect different depositional settings across a large-scale left-turning channel bend: A) Heterogeneity trends for semi-amalgamated LAP elements of Unit 1 in upstream and downstream positions. B) Unit 2 main heterogeneity, reflecting amalgamated LAPs at upstream positions and an outer-bank bar element downstream. C) Heterogeneity of upstream and downstream parts of LAPs are also recorded for Unit 3, along with adjacent transition bar deposits downstream.

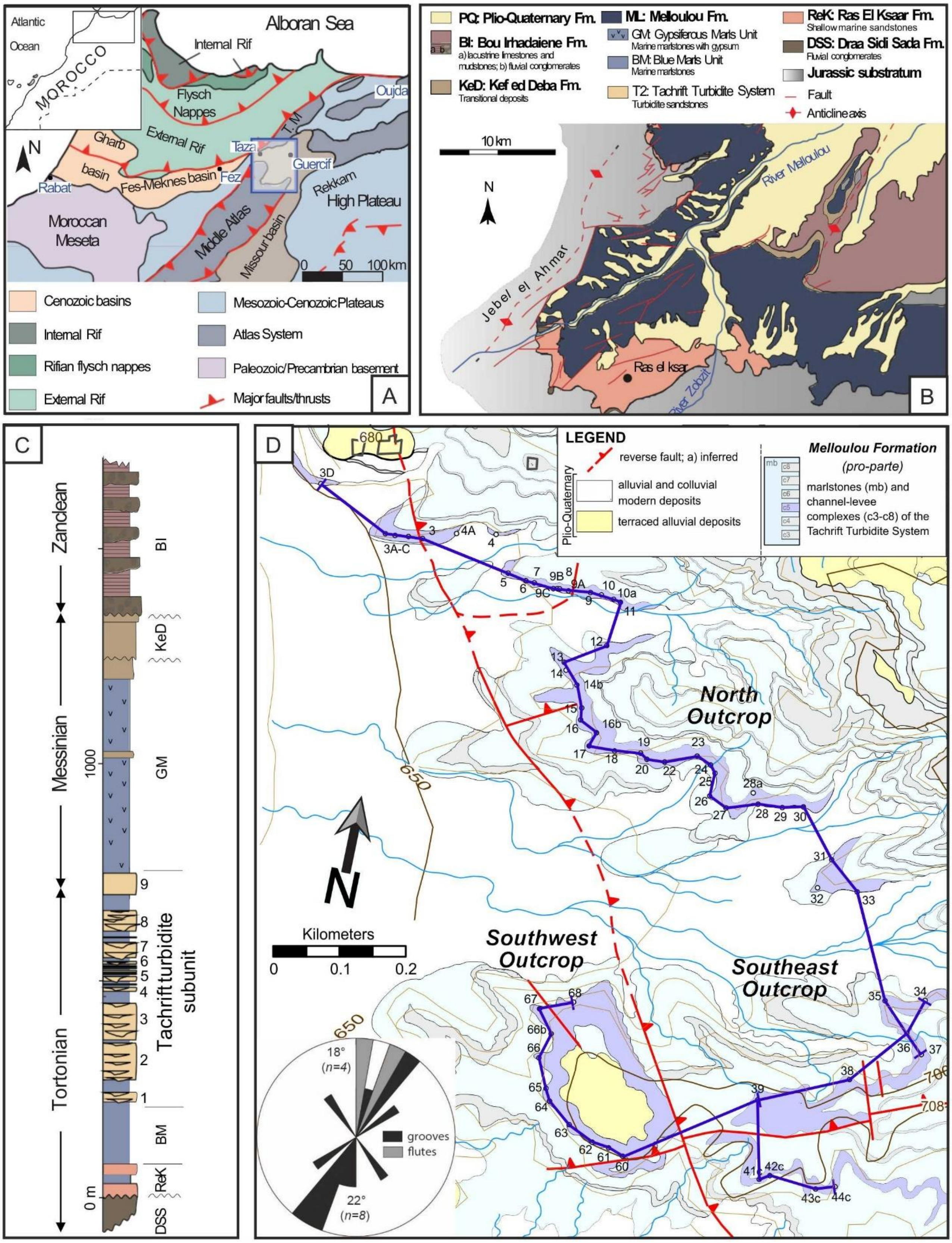
Atlantic
Ocean
MOROCCO
Alboran Sea
Internal Rif
Flysch
Nappes
External Rif
Oujda
T.M
Taza
Gharb
basin
Fes-Meknes basin
Fez
Guercif
Rabat
Rekkam
High Plateau
Moroccan
Meseta
Middle Atlas
Missour basin
0 50 100 km
Cenozoic basins
Internal Rif
Rifian flysch nappes
External Rif
Mesozoic-Cenozoic Plateaus
Atlas System
Paleozoic/Precambrian basement
Major faults/thrusts
A
PQ: Plio-Quaternary Fm.
BI: Bou Irhadaiene Fm.
a) lacustrine limestones and mudstones; b) fluvial conglomerates
KeD: Kef ed Deba Fm.
Transitional deposits
ML: Melloulou Fm.
GM: Gypsiferous Marls Unit
Marine marlstones with gypsum
BM: Blue Marls Unit
Marine marlstones
T2: Tachrift Turbidite System
Turbidite sandstones
ReK: Ras El Ksaar Fm.
Shallow marine sandstones
DSS: Draa Sidi Sada Fm.
Fluvial conglomerates
Jurassic substratum
Fault
Anticline axis
10 km
N
Jebel el Ahmar
River Melloulou
Ras el ksar
River Zobzit
B
C
Zanclean
Messinian
Tortonian
BI
KeD
GM
BM
ReK
DSS
1000
0 m
Tachrift turbidite subunit
1
2
3
4
5
6
7
8
9
D
LEGEND
reverse fault; a) inferred
Plio-Quaternary
alluvial and colluvial modern deposits
terraced alluvial deposits
Melloulou Formation (pro-parte)
marlstones (mb) and channel-levee complexes (c3-c8) of the Tachrift Turbidite System
North Outcrop
Southwest Outcrop
Southeast Outcrop
Kilometers
0 0.1 0.2
650
680
706
708
18° (n=4)
22° (n=8)
grooves
flutes

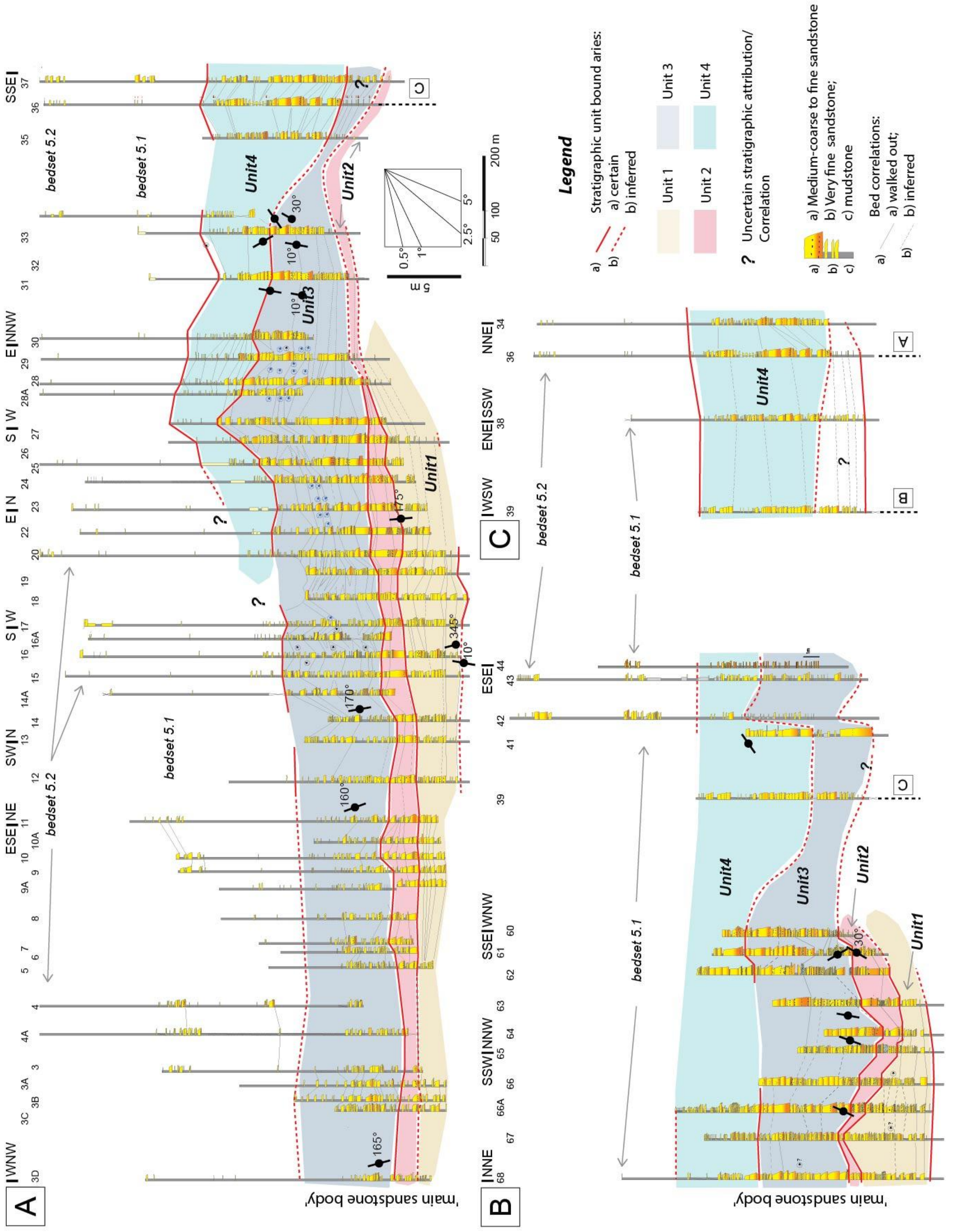
A
B
C
'main sandstone body'
bedset 5.1
bedset 5.2
Unit1
Unit2
Unit3
Unit4
Legend
Stratigraphic unit bound aries:
a) certain
b) inferred
Unit 1
Unit 2
Unit 3
Unit 4
Uncertain stratigraphic attribution/
Correlation
a) Medium-coarse to fine sandstone
b) Very fine sandstone;
c) mudstone
Bed correlations:
a) walked out;
b) inferred
5 m
200 m

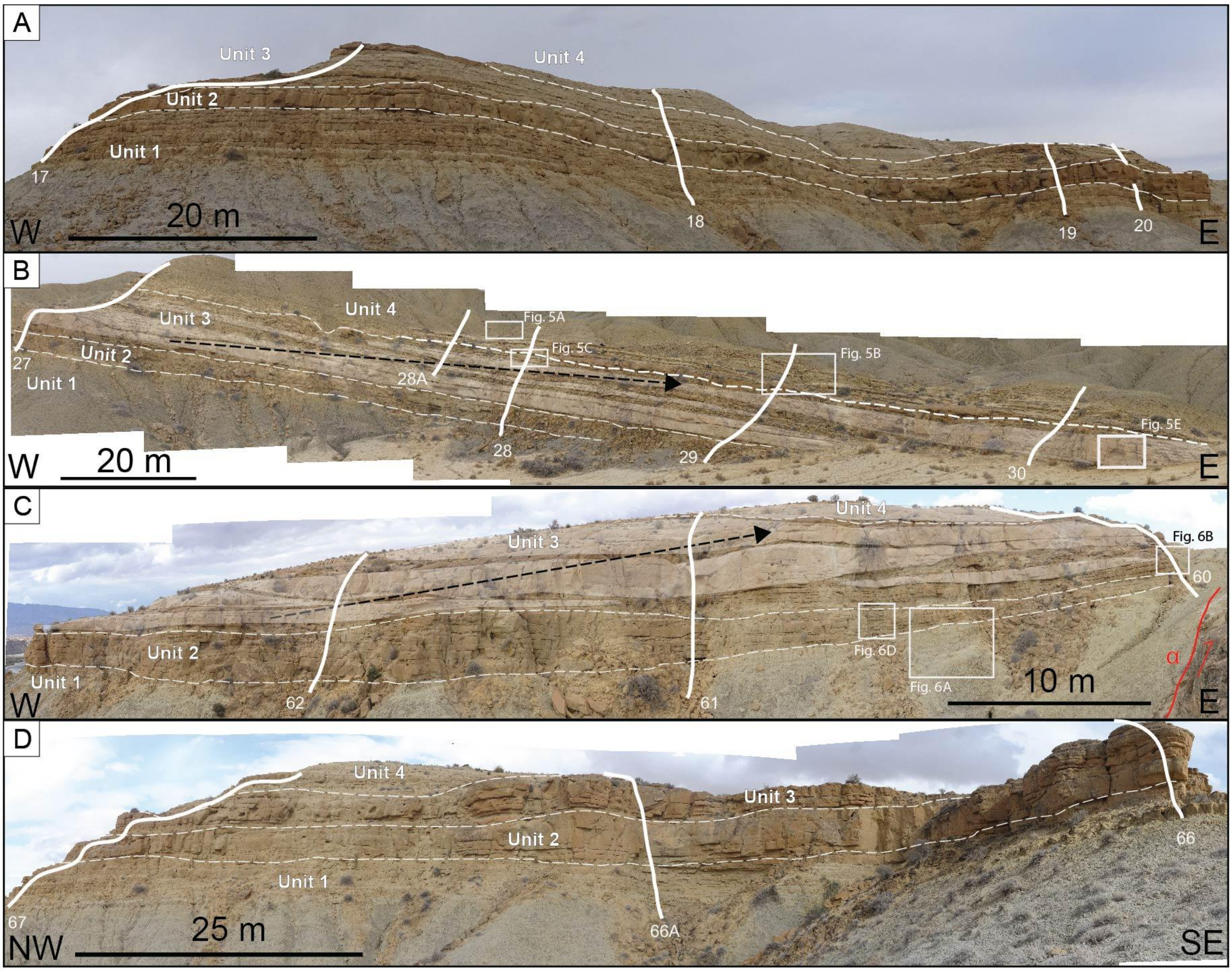
A
Unit 3
Unit 4
Unit 2
Unit 1
17
18
19
20
W
20 m
E
B
Unit 3
Unit 4
Unit 2
Unit 1
27
28A
28
29
30
Fig. 5A
Fig. 5C
Fig. 5B
Fig. 5E
W
20 m
E
C
Unit 4
Unit 3
Unit 2
Unit 1
62
61
60
Fig. 6B
Fig. 6D
Fig. 6A
10 m
α
W
E
D
Unit 4
Unit 3
Unit 2
Unit 1
67
66A
66
25 m
NW
SE

Channel-Fill Facies Associations

Panel Color	Facies Assoc. Name	Log Example	Description/Interpretation
FA1	Mudclast-rich channel-fill sandstones	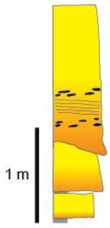	**Description:** Bedsets up to several m thick of mudclast-rich, amalgamated sandstones with basal scouring **Stratification:** Discontinuous, "cut and fill" geometries **Average Net/Gross:** 95-100% **Dominant Facies:** F1, F2, F4 **Interpretation:** Deposition at channel thalweg and/or bottomsets of bank-attached bars
FA2	Trough cross-stratified channel-fill sandstones	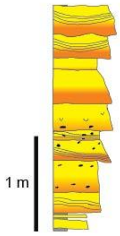	**Description:** Amalgamated thin- to medium-bedded, medium- to coarse-grained sandstones **Stratification:** Trough cross-stratified, inclined **Average Net/Gross:** ~90% **Dominant Facies:** F3, F1, F4 **Interpretation:** Bar forms of laterally accreting channel fills
FA3	Sand-rich channel-fill heterolithics	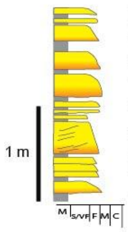	**Description:** Thin- to medium-bedded fine- to medium-grained, normally graded and structured sandstones, intercalated with thin mudstone beds **Stratification:** Trough-cross and inclined **Average Net/Gross:** ~75% **Dominant Facies:** F4, F5, F6 **Interpretation:** Heterolithic sandy channel bars
FA4	Mud-rich channel-fill heterolithics	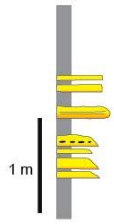	**Description:** Thin- to medium-bedded alternations of mudstones and very fine- to medium-grained sandstones with occasional mudclast presence. **Stratification:** Planar-parallel, inclined, low-angle **Average Net/Gross:** 20-25% **Dominant Facies:** F5, F4, F6 **Interpretation:** Late-stage channel infils, muddy heterolithic channel bars
FA5	Channel margin deposits	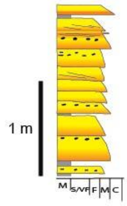	**Description:** Variously amalgamated thin- to medium-bedded, mud clast-rich sandstones **Bedding character:** Planar-parallel **Average Net/Gross:** ~85% **Dominant Facies:** F1, F5, F4 **Interpretation:** Deposition in a channel to levee transition setting

Overbank Facies Associations

Panel Color	Facies Assoc. Name	Log Example	Description/Interpretation
FA6	Proximal overbank deposits	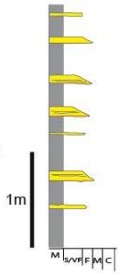	**Description:** Thin-bedded, fine-grained usually structured sandstones alternating with mudstones **Bedding Character:** Planar-parallel, **Average Net/Gross:** 15-20% **Dominant Facies:** F5, F6 **Interpretation:** Traction plus fallout overbank deposition proximal to a channel
FA7	Distal overbank deposits	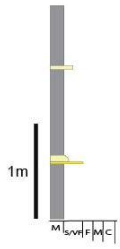	**Description:** Marlstone/mudstone with rare siltstone and very thin-bedded sandstone intercalations **Bedding Character:** Planar-parallel, **Average Net/Gross:** 0-5% **Dominant Facies:** F5, F6, F7 **Interpretation:** Hemipelagic fallout and distal overbank deposition

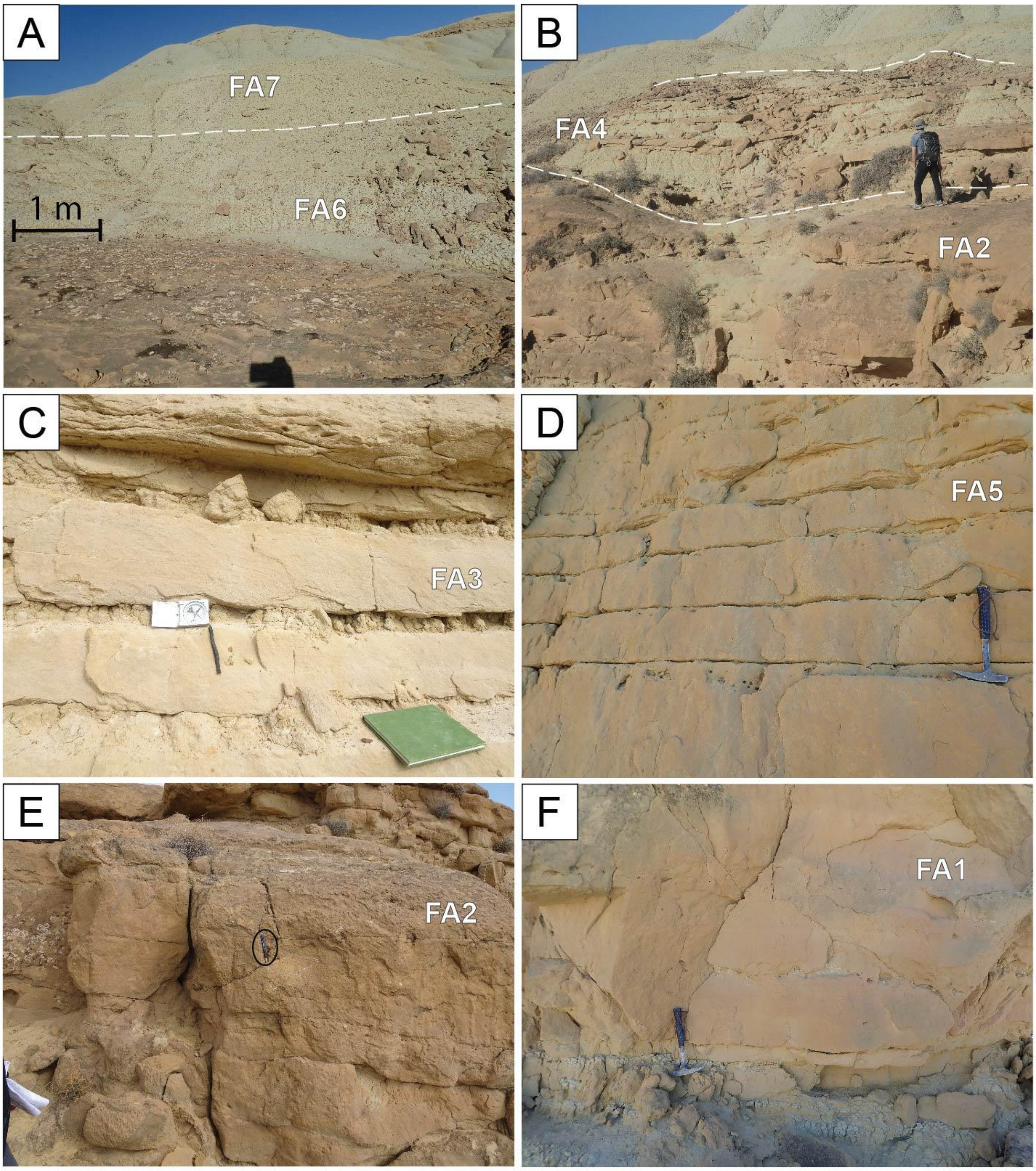
A
FA7
1 m
FA6
B
FA4
FA2
C
FA3
D
FA5
E
FA2
F
FA1

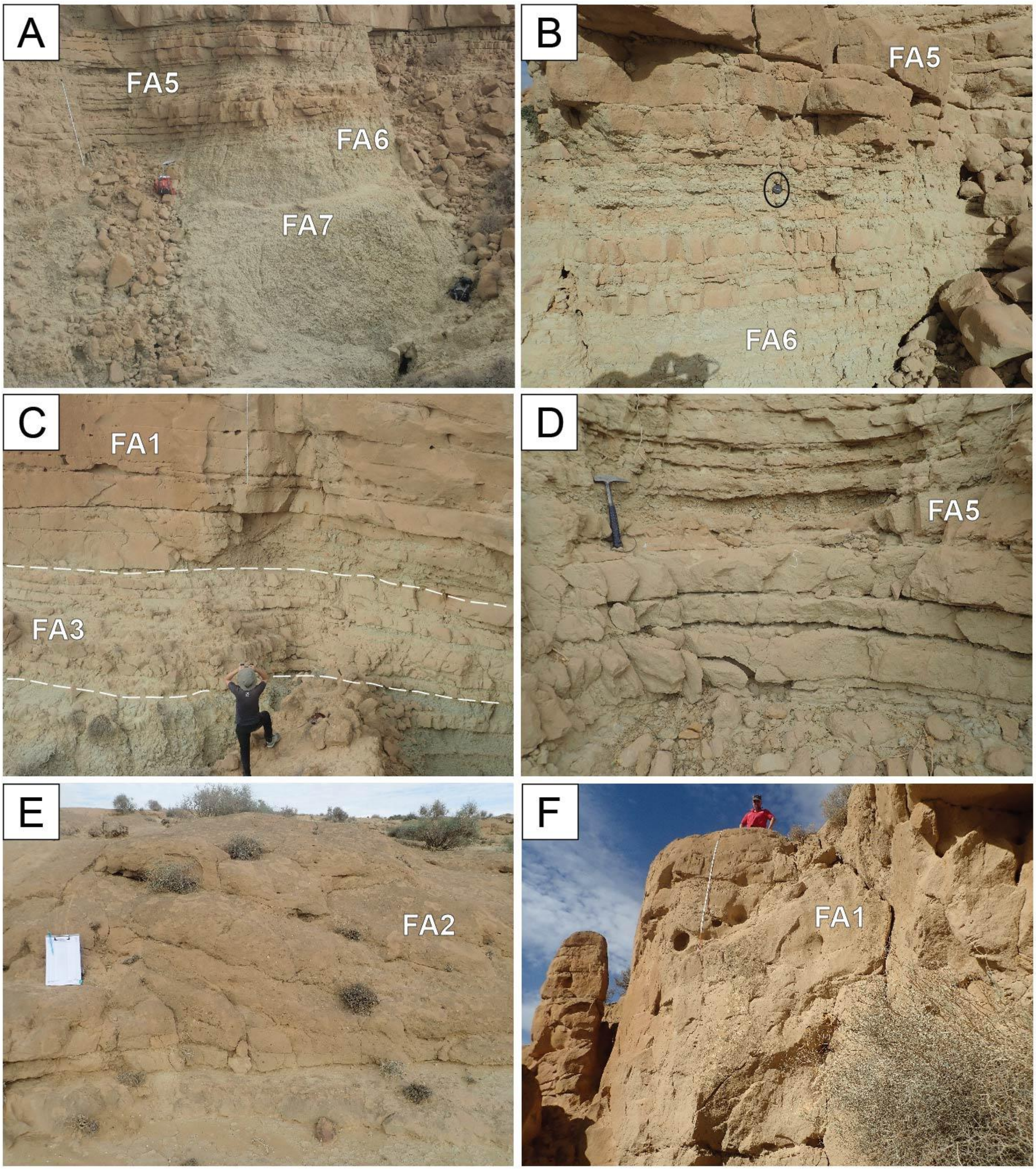
A
FA5
FA6
FA7
B
FA5
FA6
C
FA1
FA3
D
FA5
E
FA2
F
FA1

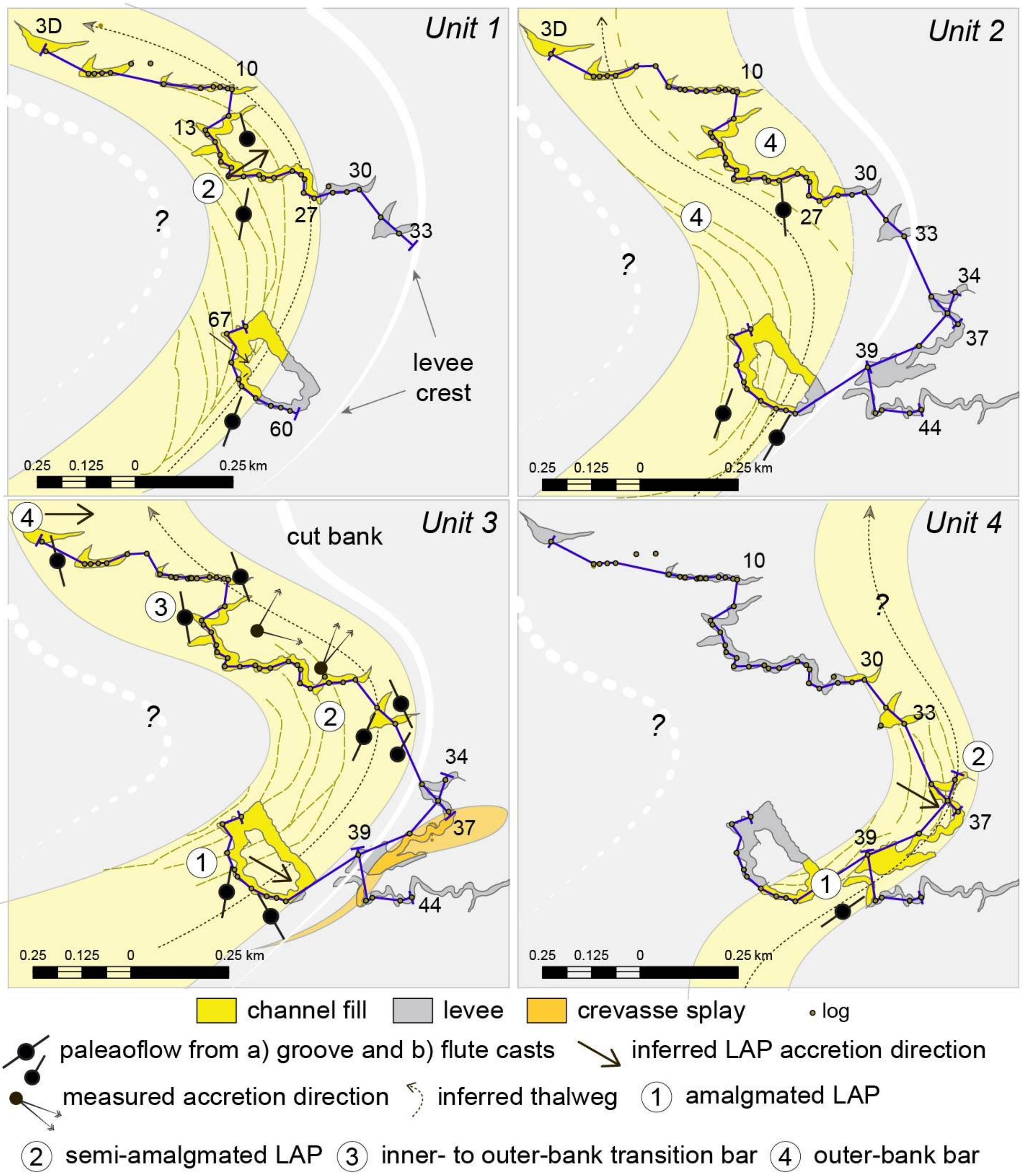
Unit 1
3D
10
13
2
30
27
33
?
67
60
levee
crest
0.25 0.125 0 0.25 km
Unit 2
3D
10
4
30
4
27
33
?
34
37
39
44
0.25 0.125 0 0.25 km
Unit 3
4
cut bank
3
2
?
34
37
39
1
44
0.25 0.125 0 0.25 km
Unit 4
10
?
30
?
33
2
37
39
1
0.25 0.125 0 0.25 km
channel fill
levee
crevasse splay
log
paleaoflow from a) groove and b) flute casts
inferred LAP accretion direction
measured accretion direction
inferred thalweg
1 amalgmated LAP
2 semi-amalgmated LAP
3 inner- to outer-bank transition bar
4 outer-bank bar

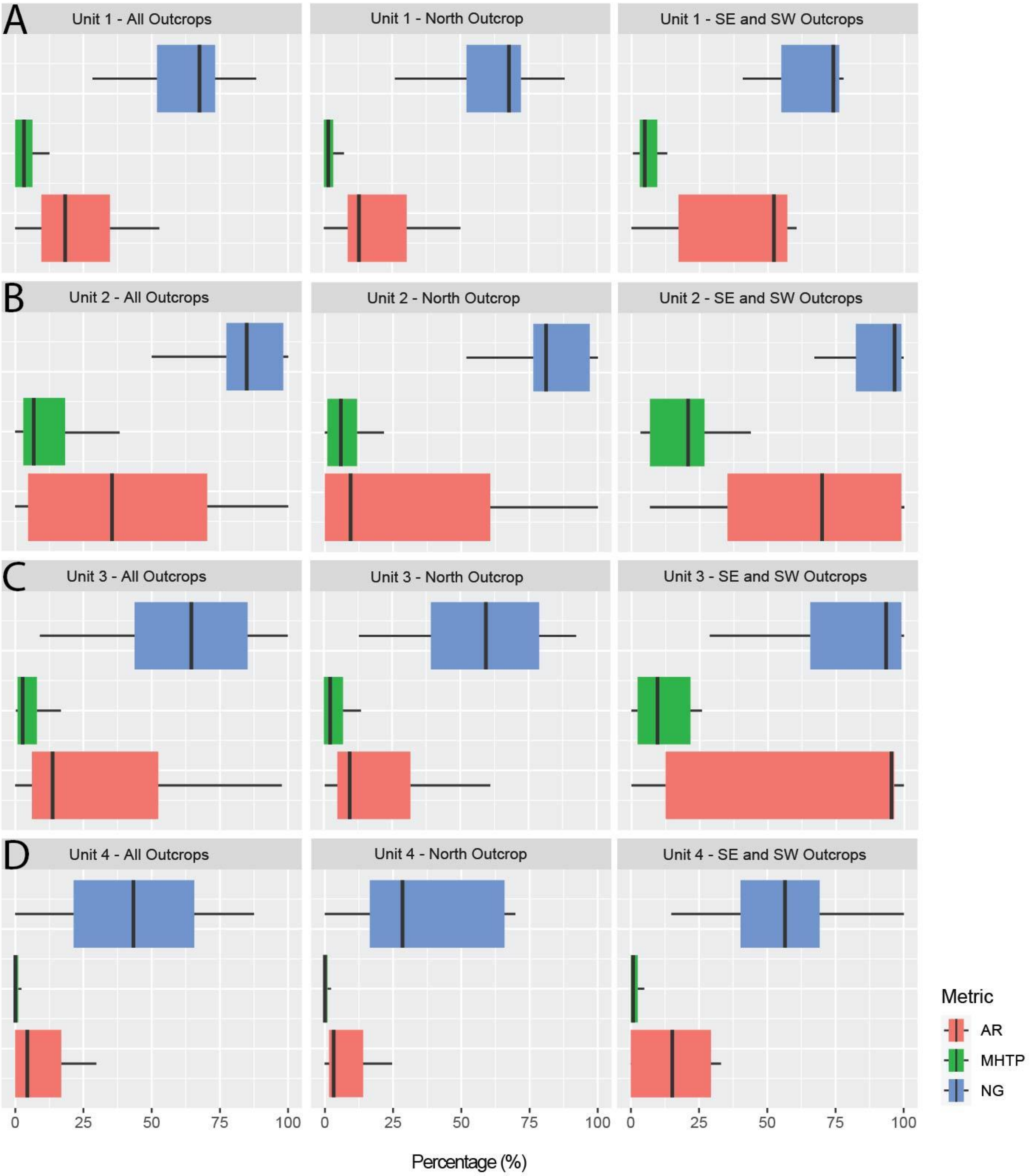

A
Unit 1 - All Outcrops
Unit 1 - North Outcrop
Unit 1 - SE and SW Outcrops
B
Unit 2 - All Outcrops
Unit 2 - North Outcrop
Unit 2 - SE and SW Outcrops
C
Unit 3 - All Outcrops
Unit 3 - North Outcrop
Unit 3 - SE and SW Outcrops
D
Unit 4 - All Outcrops
Unit 4 - North Outcrop
Unit 4 - SE and SW Outcrops
0
25
50
75
100
Percentage (%)
Metric
AR
MHTP
NG

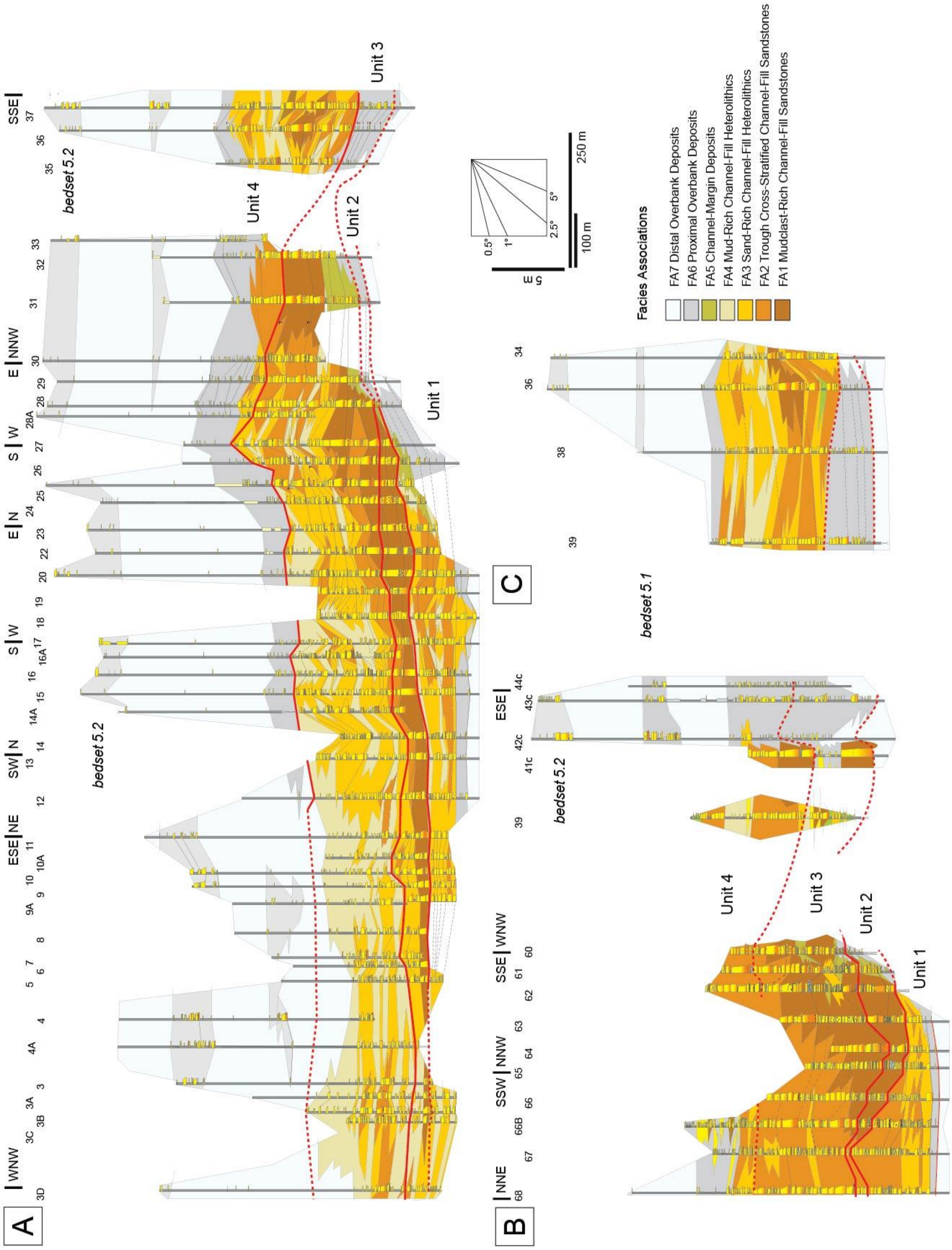

A
B
C
bedset 5.2
bedset 5.1
Unit 1
Unit 2
Unit 3
Unit 4
Facies Associations
FA7 Distal Overbank Deposits
FA6 Proximal Overbank Deposits
FA5 Channel-Margin Deposits
FA4 Mud-Rich Channel-Fill Heterolithics
FA3 Sand-Rich Channel-Fill Heterolithics
FA2 Trough Cross-Stratified Channel-Fill Sandstones
FA1 Mudclast-Rich Channel-Fill Sandstones
5 m
100 m
250 m
0.5°
1°
2.5°
5°

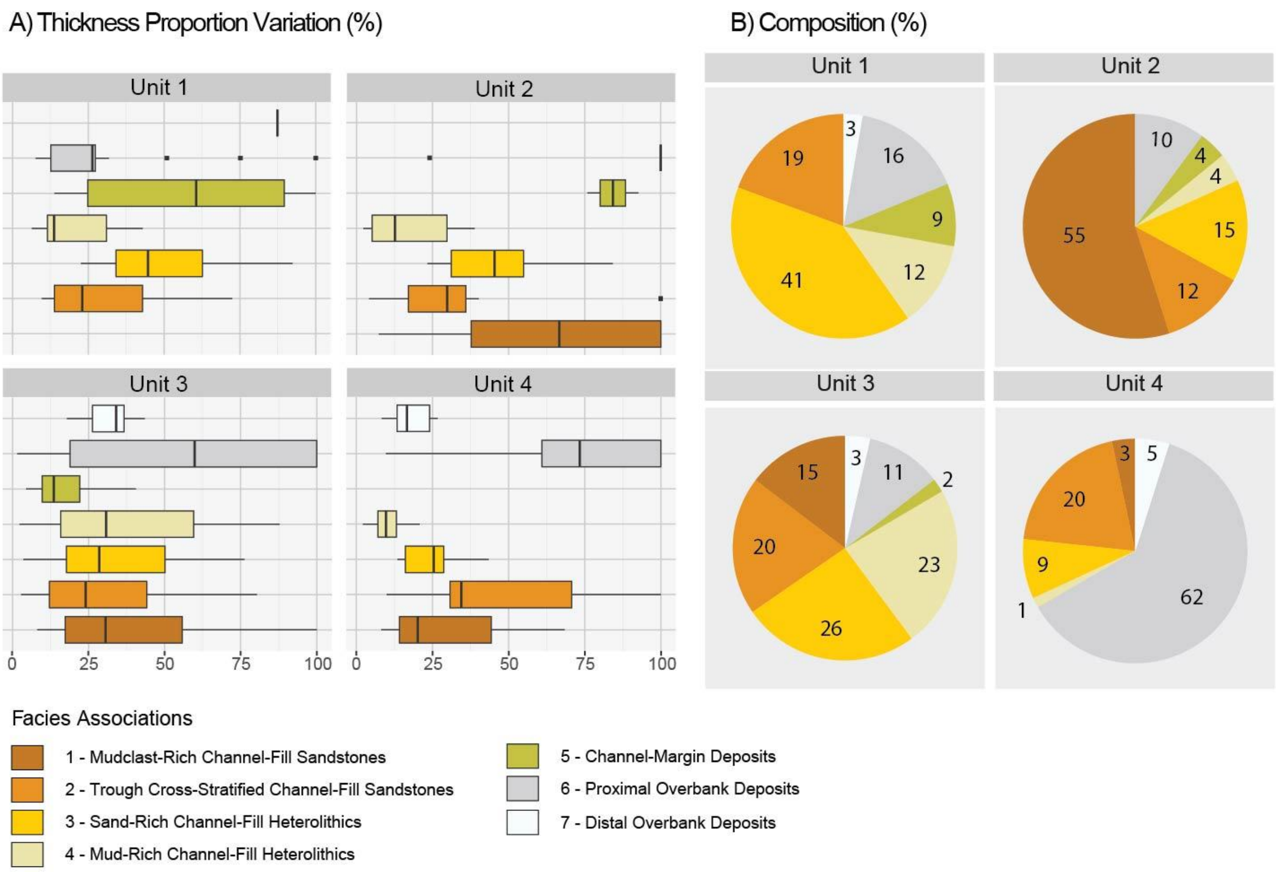
A) Thickness Proportion Variation (%)
B) Composition (%)
Unit 1
Unit 2
Unit 3
Unit 4
0
25
50
75
100
3
16
9
12
41
19
10
4
4
15
12
55
3
11
2
23
26
20
15
3
5
62
1
9
20
Facies Associations
1 - Mudclast-Rich Channel-Fill Sandstones
2 - Trough Cross-Stratified Channel-Fill Sandstones
3 - Sand-Rich Channel-Fill Heterolithics
4 - Mud-Rich Channel-Fill Heterolithics
5 - Channel-Margin Deposits
6 - Proximal Overbank Deposits
7 - Distal Overbank Deposits

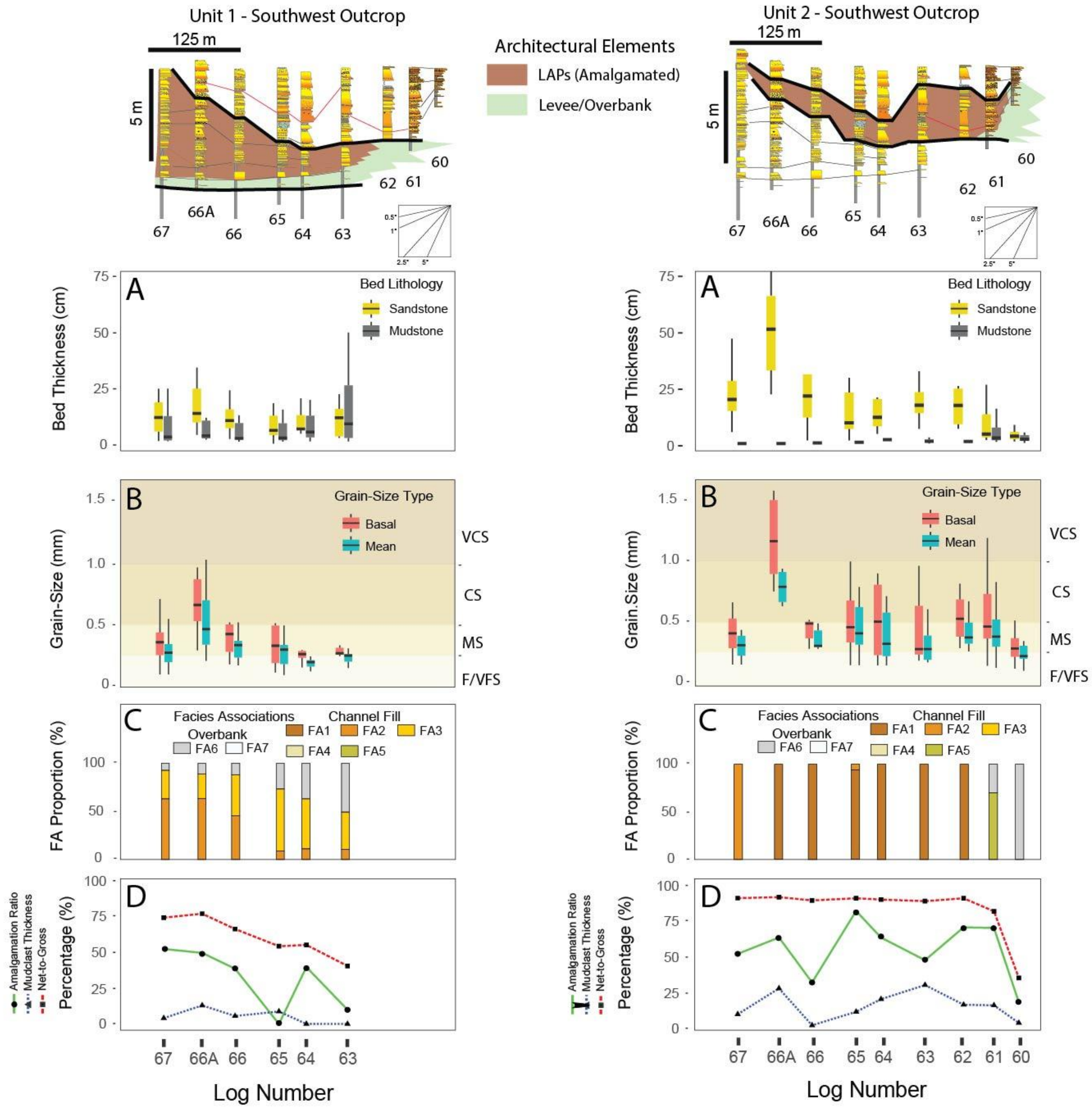

Unit 1 - Southwest Outcrop
125 m
5 m
Architectural Elements
LAPs (Amalgamated)
Levee/Overbank
Unit 2 - Southwest Outcrop
67
66A
66
65
64
63
62
61
60
Bed Lithology
Sandstone
Mudstone
Bed Thickness (cm)
Grain-Size Type
Basal
Mean
Grain-Size (mm)
VCS
CS
MS
F/VFS
Facies Associations
Overbank
Channel Fill
FA1
FA2
FA3
FA4
FA5
FA6
FA7
FA Proportion (%)
Amalgamation Ratio
Mudclast Thickness
Net-to-Gross
Percentage (%)
Log Number

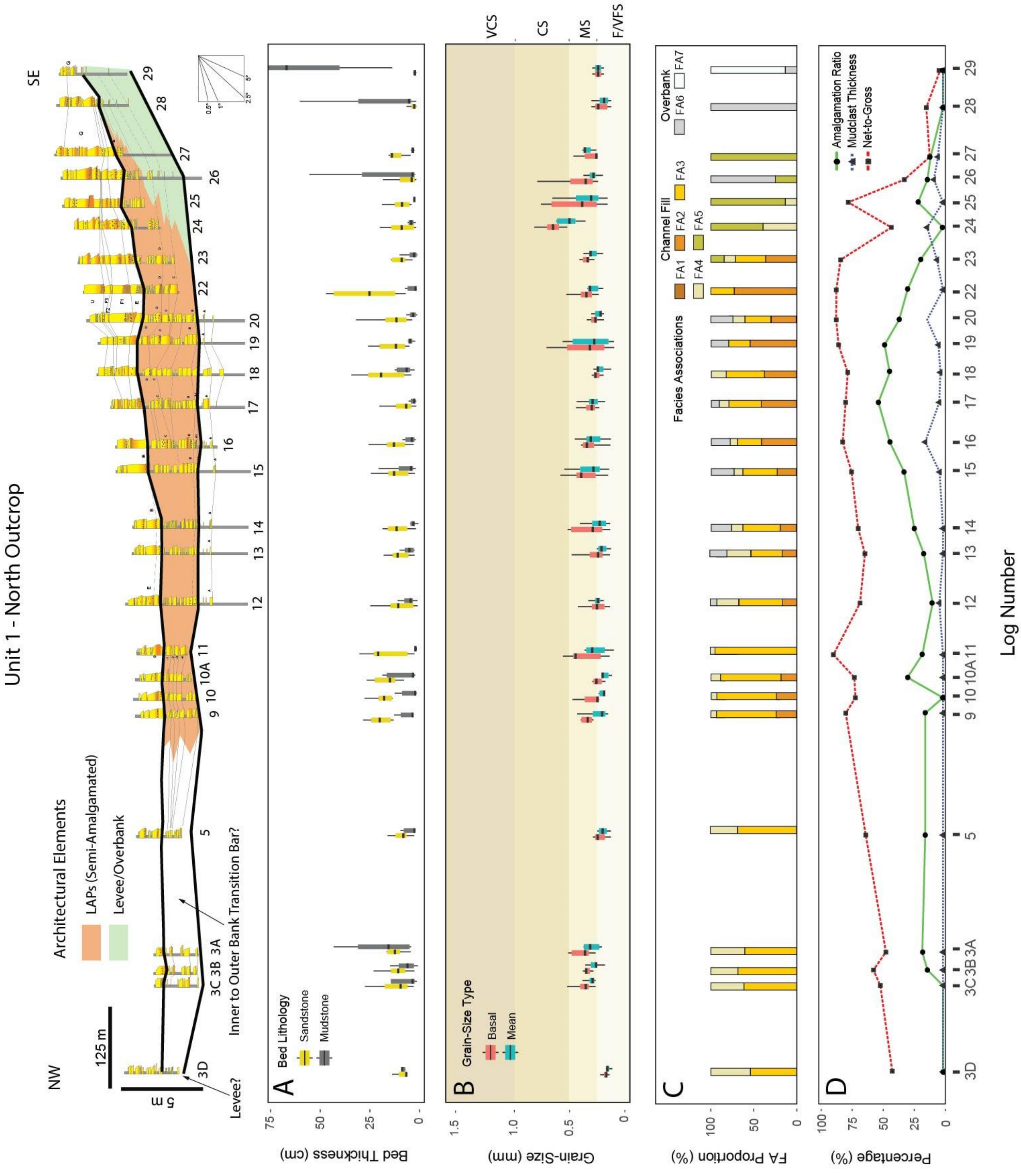

Unit 1 - North Outcrop
NW
SE
Architectural Elements
LAPs (Semi-Amalgamated)
Levee/Overbank
125 m
5 m
Levee?
Inner to Outer Bank Transition Bar?
3D
3C 3B 3A
5
9 10 10A 11
12
13
14
15
16
17
18
19
20
22
23
24
25
26
27
28
29
A
Bed Lithology
Sandstone
Mudstone
Bed Thickness (cm)
B
Grain-Size Type
Basal
Mean
Grain-Size (mm)
VCS
CS
MS
F/VFS
C
Facies Associations
Channel Fill
FA1
FA2
FA3
FA4
FA5
Overbank
FA6
FA7
FA Proportion (%)
D
Amalgamation Ratio
Mudclast Thickness
Net-to-Gross
Percentage (%)
Log Number

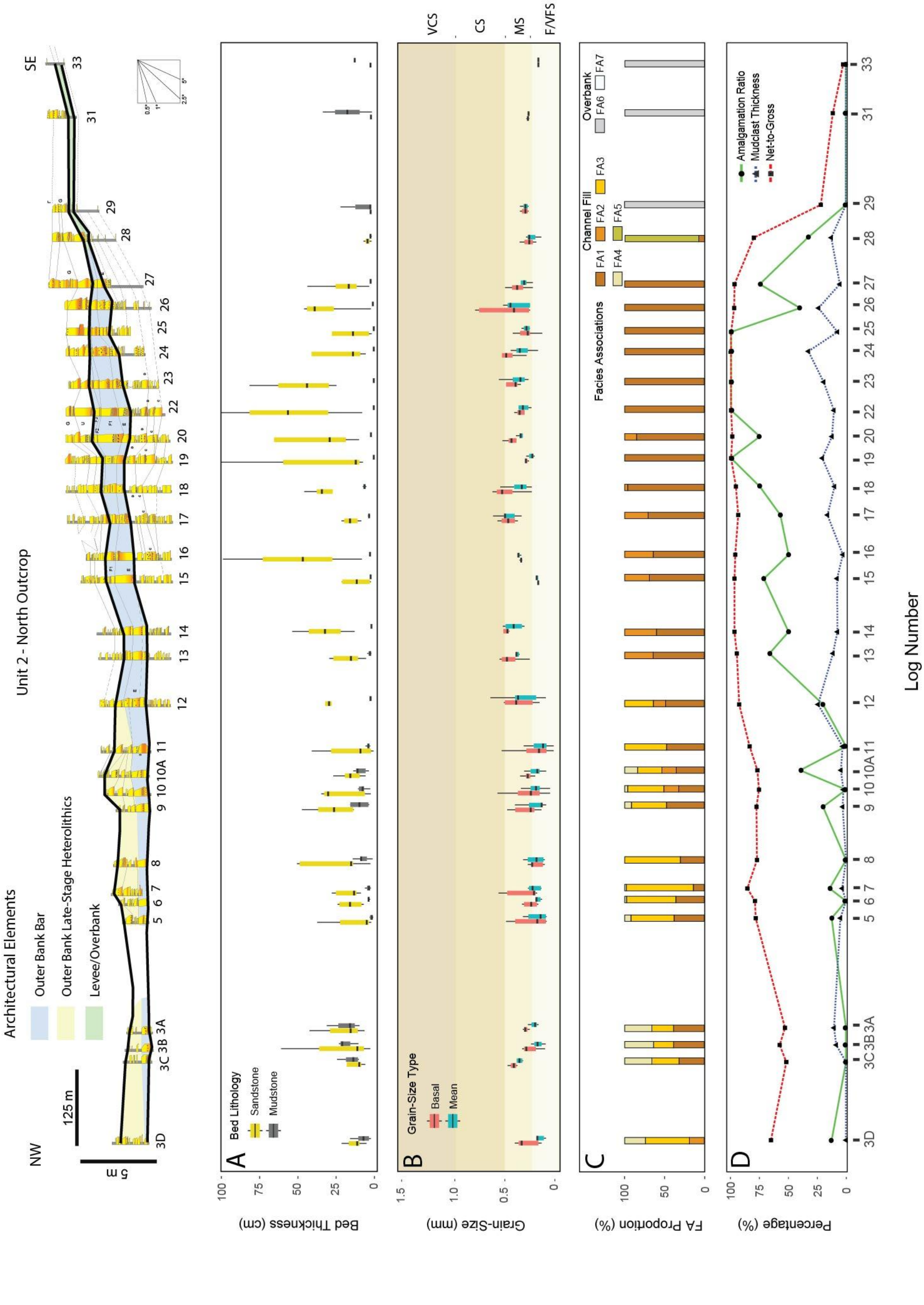
Unit 2 - North Outcrop
NW
SE
Architectural Elements
Outer Bank Bar
Outer Bank Late-Stage Heterolithics
Levee/Overbank
125 m
5 m
3D
3C 3B 3A
5 6 7
8
9 10 10A 11
12
13 14
15 16 17 18 19 20 22 23 24 25 26 27 28 29 31 33
A
Bed Lithology
Sandstone
Mudstone
Bed Thickness (cm)
100
75
50
25
0
B
Grain-Size Type
Basal
Mean
Grain-Size (mm)
1.5
1.0
0.5
0
VCS
CS
MS
F/VFS
C
Facies Associations
Channel Fill
FA1
FA2
FA3
FA4
FA5
Overbank
FA6
FA7
FA Proportion (%)
D
Amalgamation Ratio
Mudclast Thickness
Net-to-Gross
Percentage (%)
Log Number

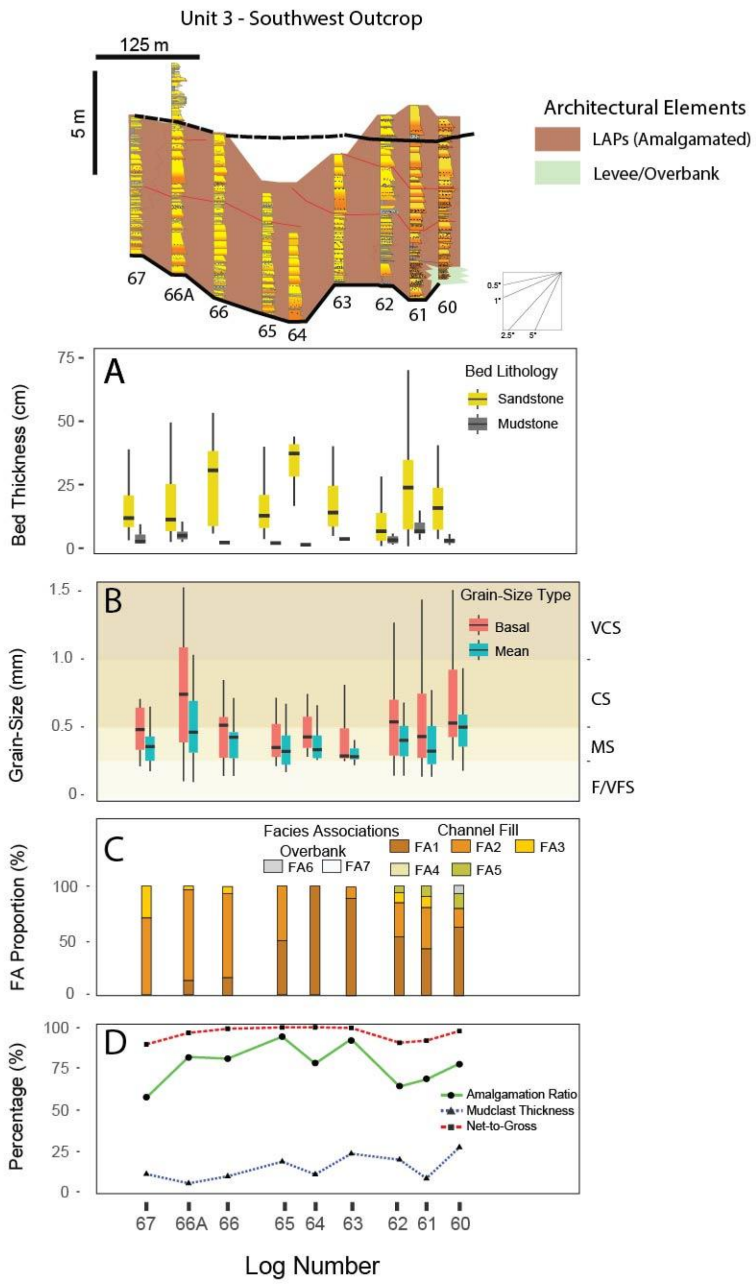
Unit 3 - Southwest Outcrop
125 m
5 m
Architectural Elements
LAPs (Amalgamated)
Levee/Overbank
67
66A
66
65
64
63
62
61
60
A
Bed Lithology
Sandstone
Mudstone
Bed Thickness (cm)
B
Grain-Size Type
Basal
Mean
Grain-Size (mm)
VCS
CS
MS
F/VFS
C
Facies Associations
Overbank
FA6
FA7
Channel Fill
FA1
FA2
FA3
FA4
FA5
FA Proportion (%)
D
Amalgamation Ratio
Mudclast Thickness
Net-to-Gross
Percentage (%)
Log Number

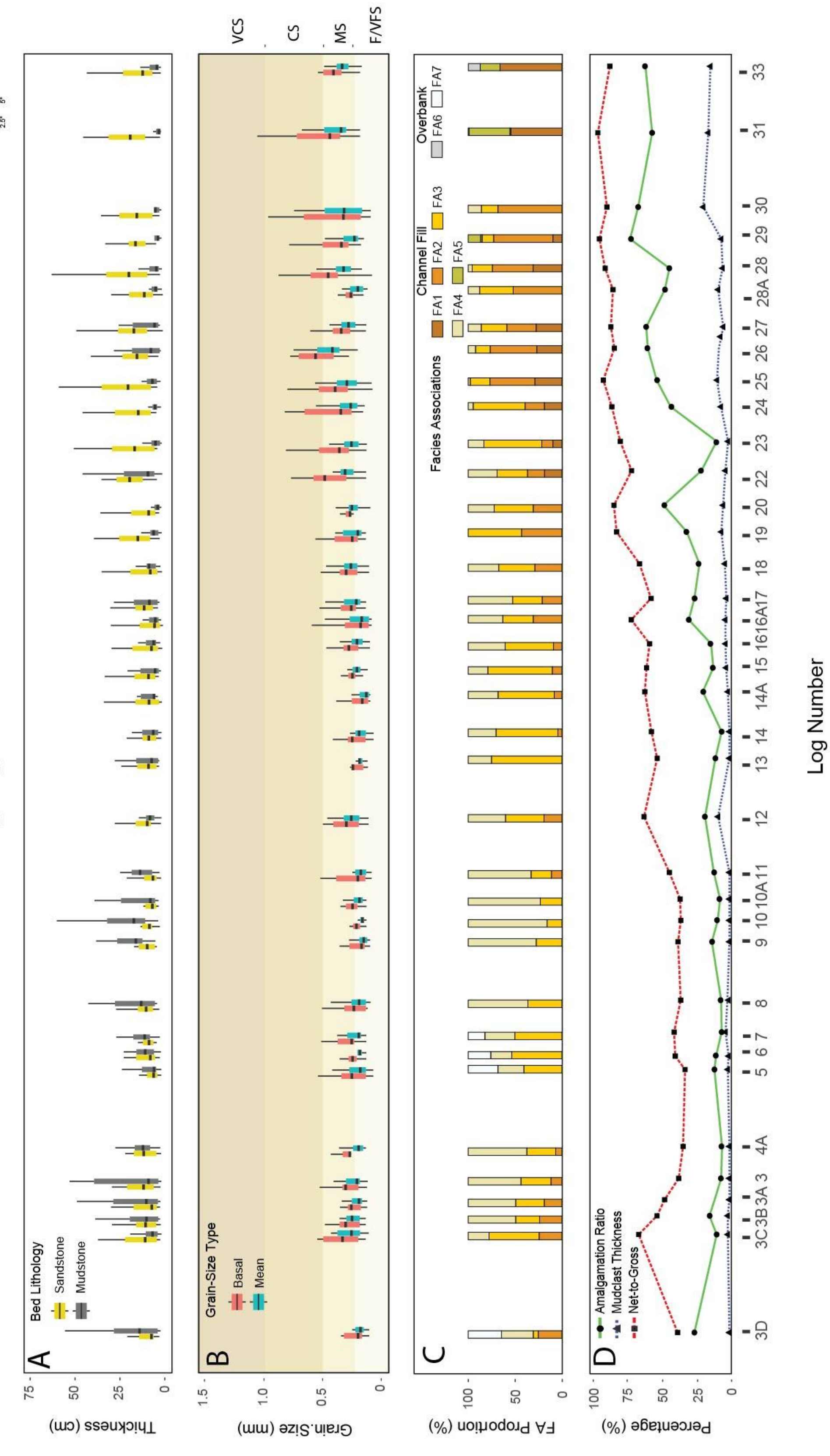
Unit 3 - North Outcrop
NW
SE
Architectural Elements
Outer Bank Bar
Levee/Overbank
LAPs (Semi-Amalgamated)
Inner to Outer Bank Transition Bar
125 m
5 m
3D
3C 3B 3A 3
4A
5 6 7
8
9 10 10A 11
12
13
14
14A
15
16
16A
17
18
19
20
22
23
24
25
26
27
28A
28
29
30
31
33
A
Bed Lithology
Sandstone
Mudstone
Thickness (cm)
B
Grain-Size Type
Basal
Mean
Grain-Size (mm)
VCS
CS
MS
F/VFS
C
Facies Associations
Channel Fill
FA1
FA2
FA3
FA4
FA5
Overbank
FA6
FA7
FA Proportion (%)
D
Amalgamation Ratio
Mudclast Thickness
Net-to-Gross
Percentage (%)
Log Number

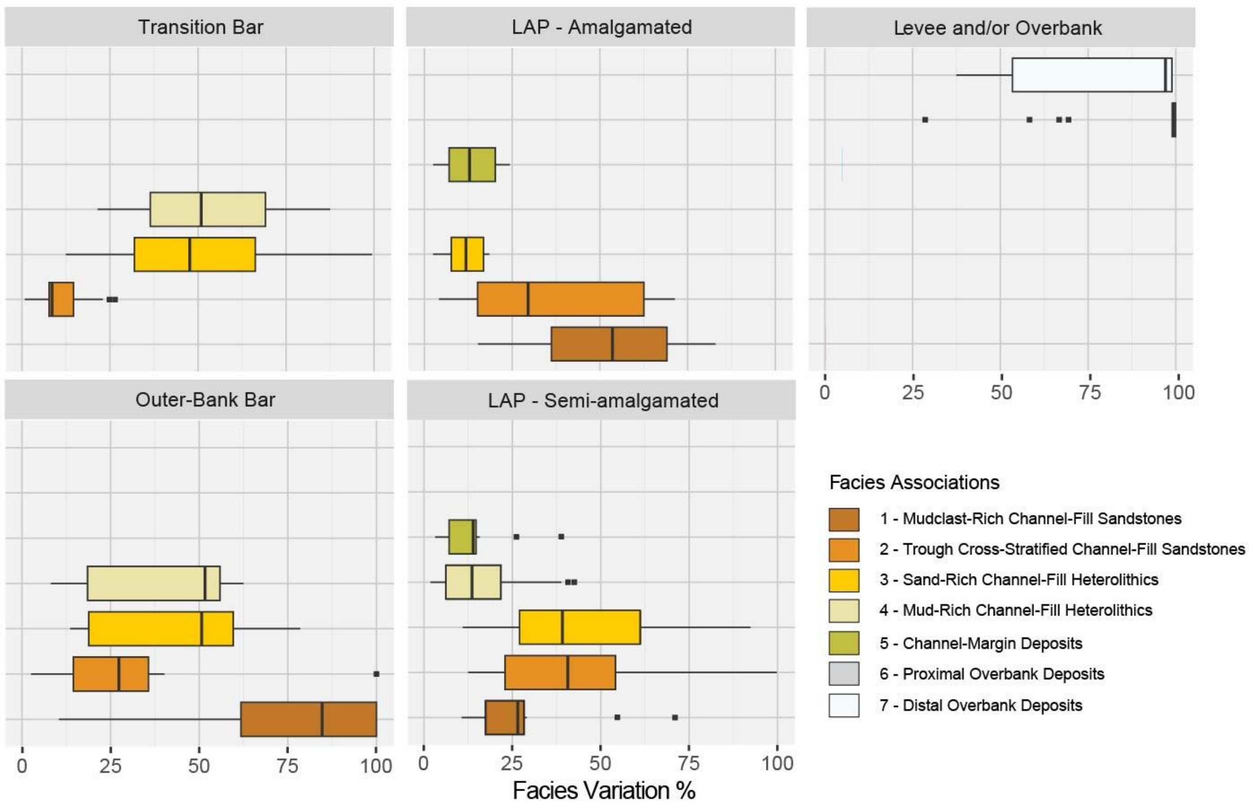
Transition Bar
LAP - Amalgamated
Levee and/or Overbank
Outer-Bank Bar
LAP - Semi-amalgamated
0
25
50
75
100
Facies Variation %
Facies Associations
1 - Mudclast-Rich Channel-Fill Sandstones
2 - Trough Cross-Stratified Channel-Fill Sandstones
3 - Sand-Rich Channel-Fill Heterolithics
4 - Mud-Rich Channel-Fill Heterolithics
5 - Channel-Margin Deposits
6 - Proximal Overbank Deposits
7 - Distal Overbank Deposits

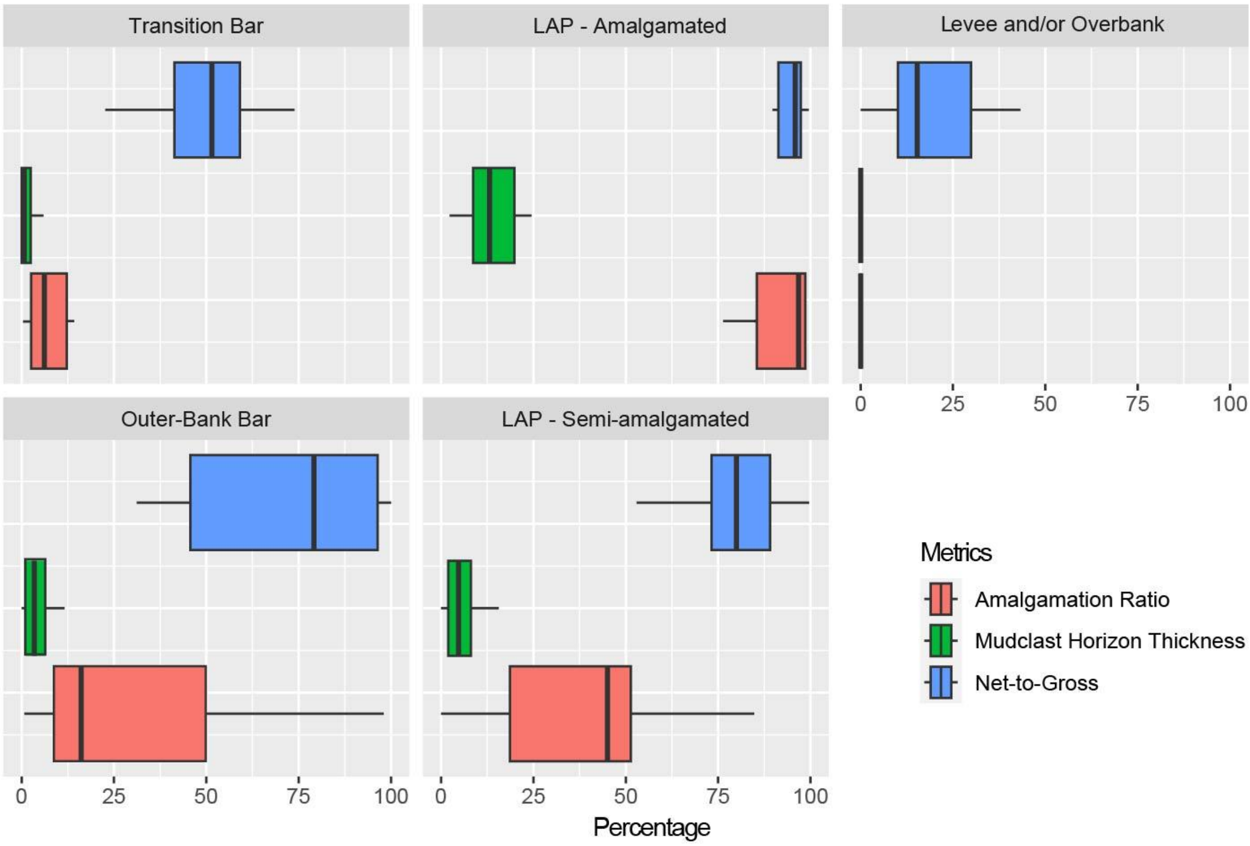
Transition Bar
LAP - Amalgamated
Levee and/or Overbank
Outer-Bank Bar
LAP - Semi-amalgamated
0
25
50
75
100
Percentage
Metrics
Amalgamation Ratio
Mudclast Horizon Thickness
Net-to-Gross

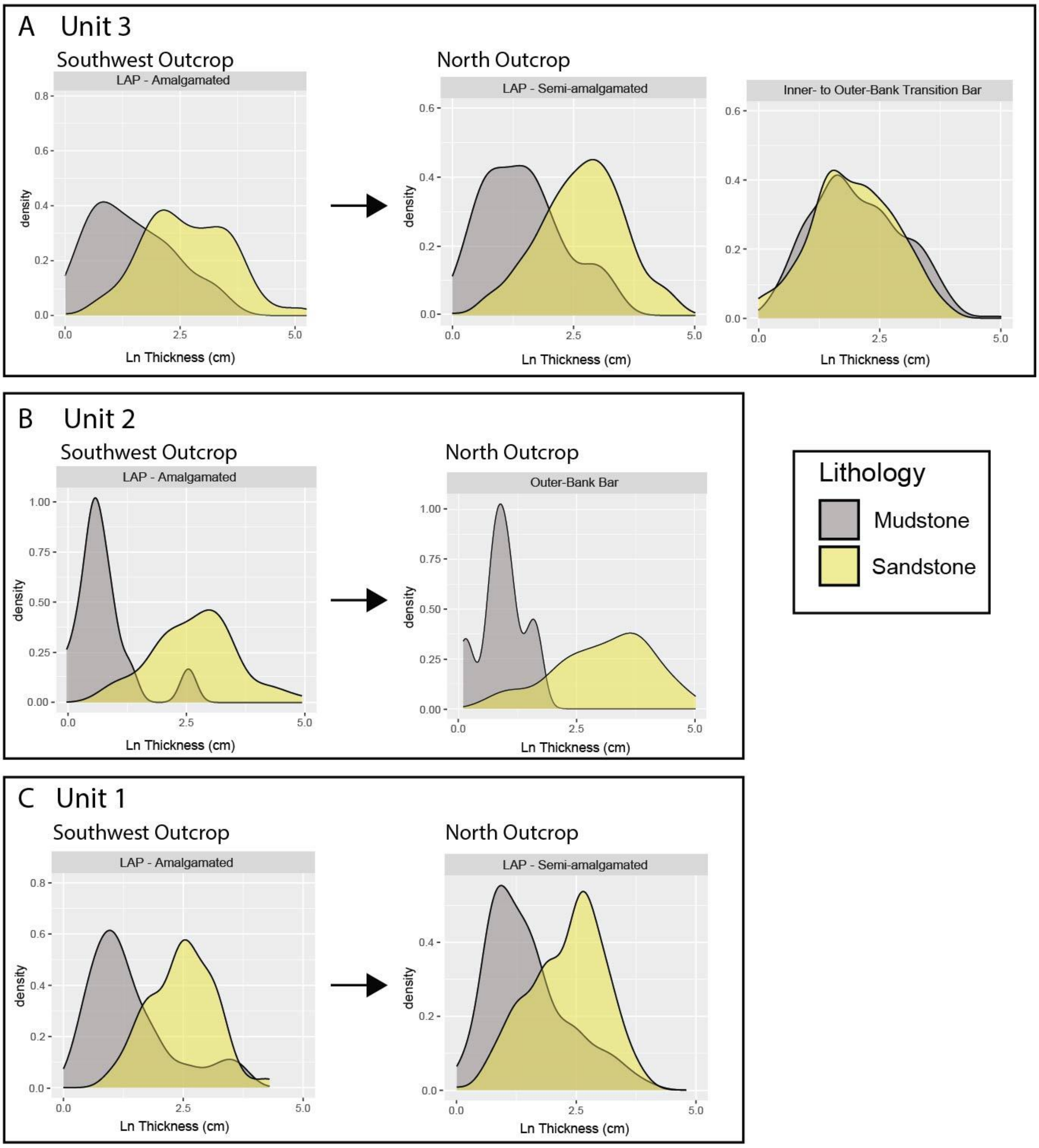
A Unit 3
Southwest Outcrop
LAP - Amalgamated
North Outcrop
LAP - Semi-amalgamated
Inner- to Outer-Bank Transition Bar
density
Ln Thickness (cm)
B Unit 2
Southwest Outcrop
LAP - Amalgamated
North Outcrop
Outer-Bank Bar
Lithology
Mudstone
Sandstone
C Unit 1
Southwest Outcrop
LAP - Amalgamated
North Outcrop
LAP - Semi-amalgamated

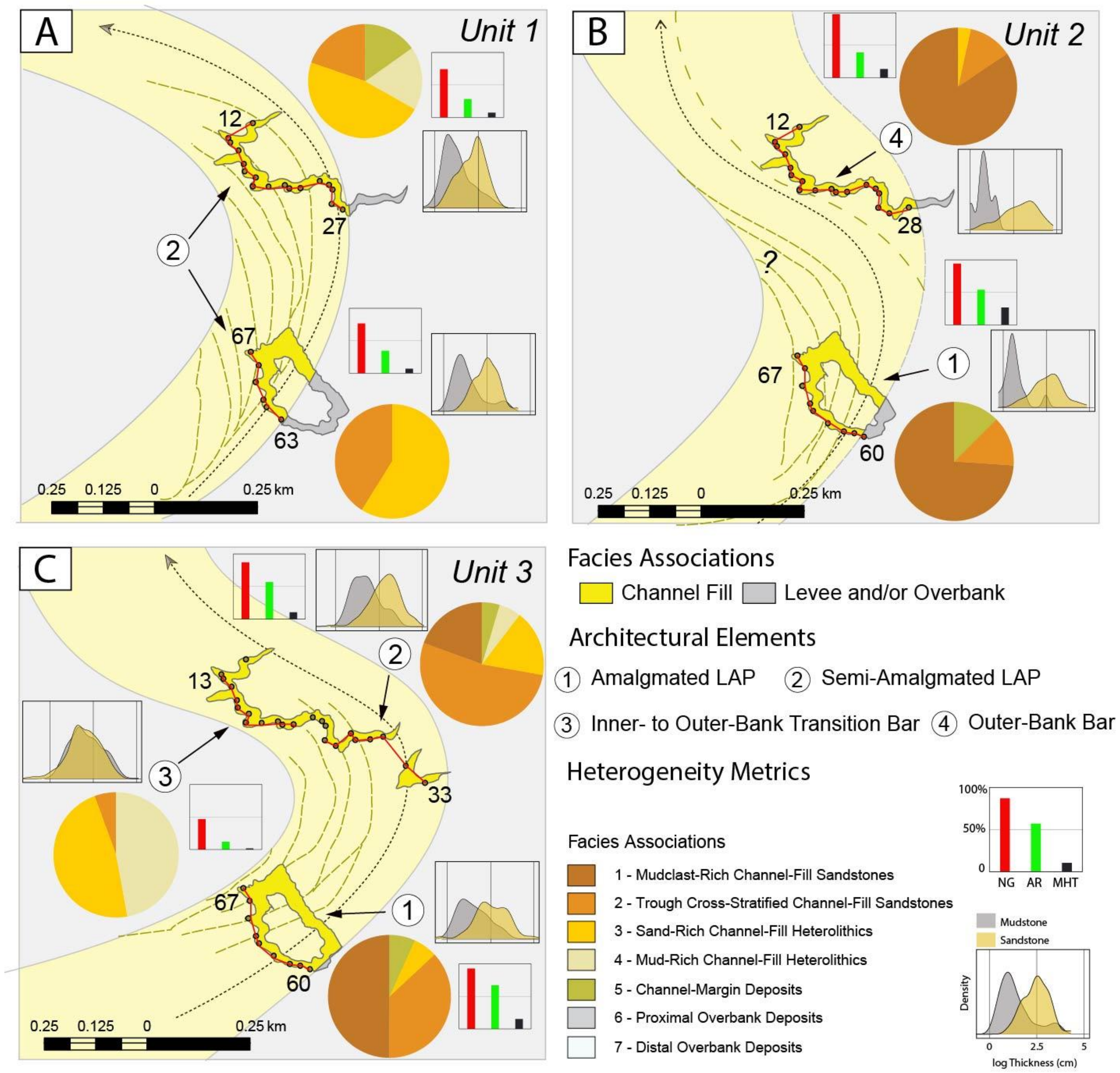

A
Unit 1
12
27
2
67
63
0.25 0.125 0 0.25 km
B
Unit 2
12
4
28
?
1
67
60
0.25 0.125 0 0.25 km
C
Unit 3
2
13
3
33
1
67
60
0.25 0.125 0 0.25 km
Facies Associations
Channel Fill
Levee and/or Overbank
Architectural Elements
1 Amalgmated LAP
2 Semi-Amalgmated LAP
3 Inner- to Outer-Bank Transition Bar
4 Outer-Bank Bar
Heterogeneity Metrics
Facies Associations
1 - Mudclast-Rich Channel-Fill Sandstones
2 - Trough Cross-Stratified Channel-Fill Sandstones
3 - Sand-Rich Channel-Fill Heterolithics
4 - Mud-Rich Channel-Fill Heterolithics
5 - Channel-Margin Deposits
6 - Proximal Overbank Deposits
7 - Distal Overbank Deposits
100%
50%
0
NG
AR
MHT
Mudstone
Sandstone
Density
0
2.5
5
log Thickness (cm)

Table 1: Sedimentary facies recognized within the studied part of Tachrift Channel Complex 5, see also Marini et al., this volume.

FACIES	FACIES NAME	GRAIN SIZE AND SORTING	SEDIMENTARY STRUCTURES AND BIOTURBATION	PROCESS INTERPRETATION	FACIES EQUIVALENTS
F1	**Mudclast-rich coarse-grained sandstone**	Medium to very coarse sand; mud clasts are up to fine cobble, subrounded; basal lags up to fine pebbles; poorly sorted	Crude normal grading; coarser lags in basal scours; inversely graded sand to granule layers close to bed base; abundant mud clasts dispersed or concentrated in the lower or in the upper part of beds, randomly oriented	Traction carpet and “en-masse” deposition from high-density turbidity currents	S1-S3 of Lowe (1982); F4 and F5 of Mutti (1992)
F2	**Mudclast breccia**	Mud clasts up to very coarse pebble, subangular to moderately rounded; matrix is medium- to very coarse-grained; very poorly sorted	Mud clasts randomly oriented	En-masse deposition from high-density flows charged with mud-clasts following interaction with levee mudstones (e.g., F6 and F7)	S1 of Lowe (1982)
F3	**Cross-stratified medium-grained sandstone**	Medium to coarse sand; mud clasts are granule to medium pebble sized; moderately sorted	Crude normal grading; low-angle cross-lamination; bioturbation moderate to absent, in the upper part of beds	Traction deposition from high-density turbidity currents	Tt of Lowe (1982); F6 of Mutti (1992)
F4	**Structureless medium- to fine-grained sandstone**	Medium to fine sand; coarser lags at base of beds; moderately well-sorted	Crude normal grading; inversely graded layers close to base of beds; rare mud clasts, concentrated in the lower or in the upper part of beds, randomly oriented; bioturbation moderate to absent, in the upper part of beds	“En-masse” deposition and traction carpets of high-density turbidity currents	T_a division of Bouma (1962); S2-S3 of Lowe (1982); F7 and F8 of Mutti (1992)
F5	**Laminated fine-grained sandstone**	Very fine to fine sand; well-sorted	Normal grading; planar-parallel, and ripple lamination; convolutions; bioturbation intense	Traction-plus-fallout deposition from waning low-density turbidity currents	T_{b-d} sequence of Bouma (1962)
F6	**Turbidite mudstone**	Clay to silt	Faintly laminated	Fallout from very diluted turbidity currents	T_e division of Bouma (1962)
F7	**Marlstone**	Clay to silt	Contains pelagic foraminifera and fragments of thin-shelled molluscs	Hemipelagic fallout	-

Table 2: Descriptive statistics of thickness and grain size for sandstone and mudstone beds across stratigraphic units of Tachrift Channel Complex 5.

	Unit Thickness (m)	Basal Grain Size (mm)		Sandstone Thickness (cm)			Mudstone Thickness (cm)		
	Max.	Max.	Ave.	Ave.	SD	n	Ave.	SD	n
All Outcrops									
Unit 4	9.4	2.1	0.297	10.4	13.9	473	17.6	27.6	388
Unit 3	11.2	3	0.356	14.6	17.2	1352	12.8	20	846
Unit 2	2.9	2	0.391	22.5	24.4	232	7.6	11.7	127
Unit 1	7.2	1.5	0.358	12.6	9.7	411	10.6	14.4	294
SW and SE Outcrops (Upstream)									
Unit 4	7.9	2.1	0.330	12.2	16.7	176	12.6	21	125
Unit 3	11.2	3	0.484	18.6	24.9	337	13.4	25.5	112
Unit 2	2.9	2	0.492	18.4	21.9	70	5.3	9.1	30
Unit 1	7.2	1.5	0.435	13.9	11.3	114	10.9	13.3	71
North Outcrop (Downstream)									
Unit 4	9.4	1.4	0.277	9.4	11.8	297	20	30	263
Unit 3	10.4	2	0.314	13.3	13.5	1015	12.7	19.1	734
Unit 2	2.5	0.9	0.347	24.2	25.3	162	8.3	12.4	97
Unit 1	4.7	1.1	0.328	12.1	9.1	297	10.4	14.8	223

Table 3: Descriptive statistics for net-to-gross (NG), amalgamation ratio (AR) and mud-clast horizon thickness percentage (MHTP), for Southwest, Southeast (upstream) and North (downstream) Outcrops of stratigraphic Units of the Tachrift Channel Complex 5.

Outcrop	**Unit**	**NG (%)**			**AR (%)**			**MHTP (%)**		
		Mean	*Sd*	*Min-Max*	*Mean*	*Sd*	*Min-Max*	*Mean*	*Sd*	*Min-Max*
SW and SE Outcrops (Upstream)										
	Unit 1	60.7	15.3	40.8-77.6	28.3	23.9	0-57.6	5.5	5.3	0-13.9
	Unit 2	84.7	25.0	25.2-99.7	68.3	35.8	0-100	22.7	14.0	3.0-43.5
	Unit 3	75.8	34.2	9.2-100	68.7	46.5	0-100	11.6	9.4	0-25.8
	Unit 4	64.0	32.5	16.5-100	41.0	45.5	0-100	5.5	10.0	0-29.9
North Outcrop (Downstream)										
	Unit 1	60.1	21.3	3.9-89.4	13.8	13.4	0-48.4	2.9	5.2	0-24.2
	Unit 2	79.4	26.1	2.5-100	40.6	42.0	0-100	7.6	9.5	0-44.9
	Unit 3	56.5	23.0	11.4-93.4	20.7	25.6	0-100	3.5	4.6	0-17.7
	Unit 4	25.7	22.8	0-72.2	10.4	22.6	0-100	0.9	1.9	0-6.0

Table 4: Mean values for heterogeneity metrics for architectural elements observed. Bold numbers highlight higher values characterizing specific elements. Abbreviations: net-to-gross (NG), amalgamation ratio (AR) and mud-clast horizon thickness percentage (MHTP).

Facies Associations	**Architectural Elements**	**Sub-elements**	**Sandstone Thickness (cm)**		**Mudstone Thickness (cm)**		**Basal Grain Size**	**NG %**	**AR %**	**MHT %**
			m	**sd**	**m**	**sd**				
Channel-Fill	**Lateral-Accretion Package**	Amalgamated	19.9	23.3	6.2	7.9	**cS**	**91.8**	**92.2**	**15.3**
		Semi-Amalgamated	16.9	15.1	6.9	8.1	mS	80.4	41.3	6.1
	Inner- to Outer-Bank Transition Bar	n/a	9.8	8.9	11.9	13.4	fS	50.7	6.9	1.7
	Outer-Bank Bar	n/a	**22.1**	**23.6**	14.2	21.6	mS	70.4	35.4	4.8
Overbank	**Levee and/or Overbank**	n/a	4.8	5.2	**24.5**	**35.7**	fS	20.2	1.7	1.2

Table 5: Mean values for facies associations (FA) thickness proportions for architectural elements observed. Bold numbers highlight the 2 main FAs dominating within each element.

Facies Associations	Architectural Elements	Sub-Elements	FA1 %	FA2 %	FA3 %	FA4 %	FA5 %	FA6 %	FA7 %
Channel-Fill	**Lateral-Accretion Package**	Amalgamated (Upcurrent)	**39.6**	**36.2**	12.6	0	11.6	0	0
		Semi-Amalgamated (Downcurrent)	22.2	**32.7**	**25.5**	9.8	9.8	0	0
	Inner- to Outer-Bank Transition Bar	n/a	0	10.0	**44.6**	**45.4**	0	0	0
	Outer-Bank Bar	n/a	**35.5**	14.5	20.5	**29.5**	0	0	0
Overbank	**Levee and/or Overbank**	n/a	0	0	0	0	0	**53.4**	**46.6**

Table 6: Mean values of heterogeneity metrics for upstream and downstream outcrops of Units 1 to 3. Abbreviations: IOBTB - Inner to Outer Bar Transition Bar, LAPs - Lateral Accretion Packages, LV – Levee, OBB – Outer Bank Bar, NG – Net-to-Gross, AR - Amalgamation Ratio, MHTP – Mudclast Horizon Thickness Percentage, FA – Facies Association.

Arch. Element	Elem. Thickness	Bed Thickness (cm)		SD Bed Thickness		NG %	AR %	MHTP %	FA1 %	FA2 %	FA3 %	FA4 %	FA5 %	FA6 %	FA7 %
		Sand.	Mud.	Sand.	Mud.										
Unit 3 Upstream															
IOBTB	n/a	n/a	n/a	n/a	n/a	n/a	n/a	n/a	n/a	n/a	n/a	n/a	n/a	n/a	n/a
LAPs	6.1	21.8	6.6	26.8	7	93.1	67	15.1	51.0	38.0	7.3	0	3.7	0	0
LV	3.6	4.8	19.8	6.5	33.7	31.2	10.7	7.9	0	0	0	0	0	89.1	10.9
OBB	n/a	n/a	n/a	n/a	n/a	n/a	n/a	n/a	n/a	n/a	n/a	n/a	n/a	n/a	n/a
Unit 3 Downstream															
IOBTB	2.3	9	13.2	6.5	10.7	41.7	7.5	0.6	0	5.6	47.3	47.1	0	0	0
LAPs	5.6	14.9	8.4	15.1	8.8	74.3	34.7	6	19.4	52.8	17.4	5.8	4.6	0	0
LV	1.6	5.5	32.5	4.2	38.7	15.8	3.4	0.9	0	0	0	0	0	56.3	43.7
OBB	n/a	n/a	n/a	n/a	n/a	n/a	n/a	n/a	n/a	n/a	n/a	n/a	n/a	n/a	n/a
Unit 2 Upstream															
IOBTB	n/a	n/a	n/a	n/a	n/a	n/a	n/a	n/a	n/a	n/a	n/a	n/a	n/a	n/a	n/a
LAPs	1.6	21.1	2.7	22.9	2.9	94.1	53.8	26.2	73.9	13.6	12.5	0	0	0	0
LV	0.8	4.1	7.7	1.8	11.8	28.3	0	1.5	0	0	0	0	0	100	0
OBB	n/a	n/a	n/a	n/a	n/a	n/a	n/a	n/a	n/a	n/a	n/a	n/a	n/a	n/a	n/a
Unit 2 Downstream															
IOBTB	n/a	n/a	n/a	n/a	n/a	n/a	n/a	n/a	n/a	n/a	n/a	n/a	n/a	n/a	n/a
LAPs	n/a	n/a	n/a	n/a	n/a	n/a	n/a	n/a	n/a	n/a	n/a	n/a	n/a	n/a	n/a
LV	0.5	3.8	19.8	3.2	35.2	29.4	0	4.6	0	0	0	0	0	100	0
OBB	1.1	32.9	2.8	29.5	1.3	98.4	24.3	9	84.4	12.1	3.5	0	0	0	0
Unit 1 Upstream															
IOBTB	n/a	n/a	n/a	n/a	n/a	n/a	n/a	n/a	n/a	n/a	n/a	n/a	n/a	n/a	n/a
LAPs	3.2	14.8	6.72	11.3	9.2	76.2	34.1	6.5	0	41.1	58.9	0	0	0	0
LV	0.7	3.5	29.7	2.1	12.5	7.7	0	0	0	0	0	0	0	100	0
OBB	n/a	n/a	n/a	n/a	n/a	n/a	n/a	n/a	n/a	n/a	n/a	n/a	n/a	n/a	n/a
Unit 1 Downstream															
IOBTB	n/a	n/a	n/a	n/a	n/a	n/a	n/a	n/a	n/a	n/a	n/a	n/a	n/a	n/a	n/a
LAPs	2	12.9	7.3	9.2	9.2	70.5	21.9	4.2	0	19.7	47.1	18.0	15.2	0	0
LV	1.1	5.3	27.1	4.1	25	17.5	0	0	0	0	0	0	0	92.1	7.9
OBB	n/a	n/a	n/a	n/a	n/a	n/a	n/a	n/a	n/a	n/a	n/a	n/a	n/a	n/a	n/a